iScience

CellPress
OPEN ACCESS

Article

Ischemic Stroke Impacts the Gut Microbiome, Ileal Epithelial and Immune Homeostasis

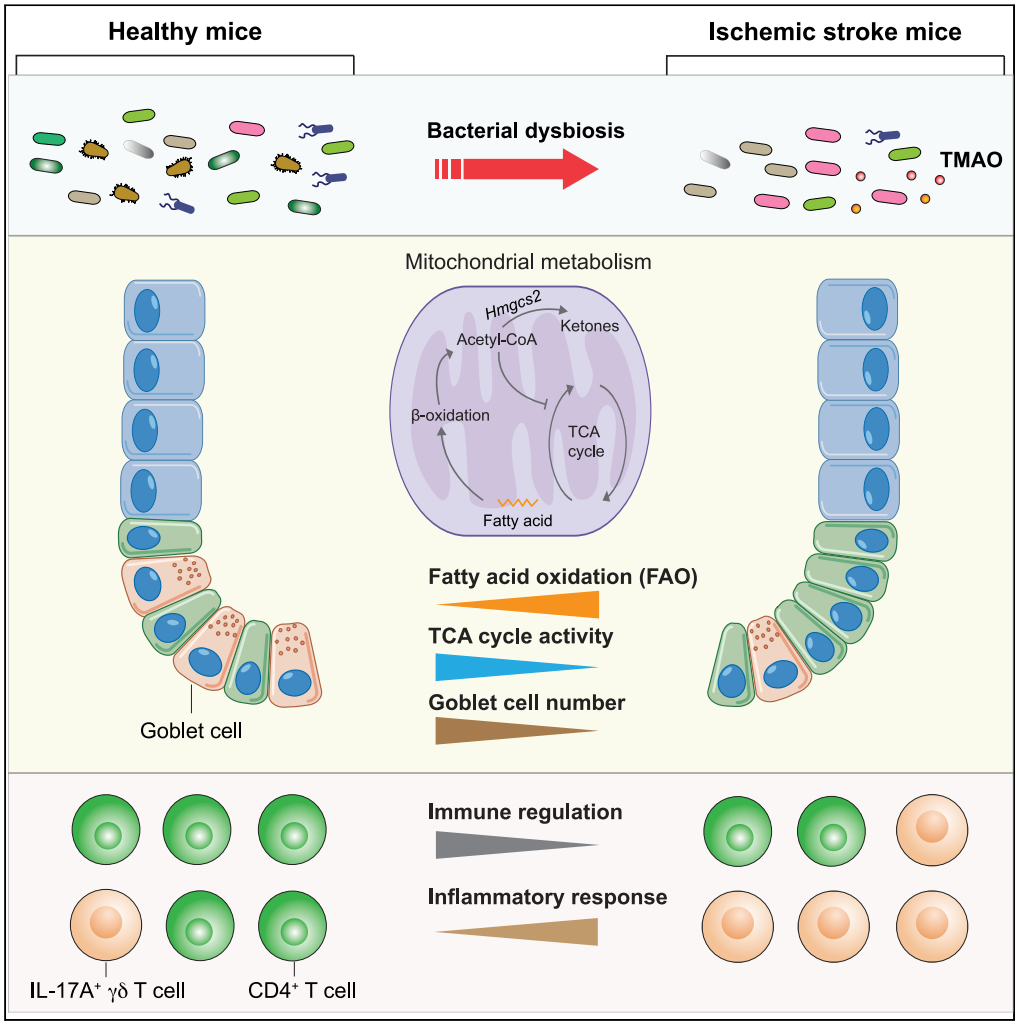

Yong Ge, Mojgan Zadeh, Changjun Yang, Eduardo Candelario-Jalil, Mansour Mohamadzadeh

zadehm@uthscsa.edu

Highlights

Stroke impairs the gut microbiome and associated metabolic circuits

Mitochondrial FAO and TCA cycle are dysregulated in iECs of poststroke mice

Stroke is associated with alterations in the ileal epithelial cell structure

Ge et al., iScience 25, 105437
November 18, 2022
https://doi.org/10.1016/j.isci.2022.105437

iScience

CellPress
OPEN ACCESS

Article

Ischemic Stroke Impacts the Gut Microbiome, Ileal Epithelial and Immune Homeostasis

Yong Ge,[1,2] Mojgan Zadeh,[1,2] Changjun Yang,[3] Eduardo Candelario-Jalil,[3] and Mansour Mohamadzadeh[1,2,4,*]

SUMMARY

Ischemic stroke critically impacts neurovascular homeostasis, potentially resulting in neurological disorders. However, the mechanisms through which stroke-induced inflammation modifies the molecular and metabolic circuits, particularly in ileal epithelial cells (iECs), currently remain elusive. Using multiomic approaches, we illustrated that stroke impaired the ileal microbiome and associated metabolites, leading to increased inflammatory signals and altered metabolites, potentially deteriorating the iEC homeostasis. Bulk transcriptomic and metabolomic profiling demonstrated that stroke enhanced fatty acid oxidation while reducing the tricarboxylic acid (TCA) cycle in iECs within the first day after stroke. Intriguingly, single-cell RNA sequencing analysis revealed that stroke dysregulated cell-type-specific gene responses within iECs and reduced frequencies of goblet and tuft cells. Additionally, stroke augmented interleukin-17A$^+$ $\gamma\delta$ T cells but decreased CD4$^+$ T cells in the ileum. Collectively, our findings provide a comprehensive overview of stroke-induced intestinal dysbiosis and unveil responsive gene programming within iECs with implications for disease development.

INTRODUCTION

Ischemic stroke occurs as a result of insufficient cerebral blood flow to the brain resulting in irreversible tissue injury and neurological deficits or death.[1] It accounts for approximately 85% of all strokes, while the other 15% are hemorrhagic in nature.[1] Over the last 30 years, clinicians and investigators have made major advances in stroke prevention and management. The widespread use of secondary prophylactic measures, such as antiplatelets, statins, and anticoagulants, as well as surgical and endovascular management of carotid stenosis, acute large-vessel occlusions, and other intracranial and cervical vascular disorders, has dramatically reduced stroke incidence.[2–4] However, despite such medical advances, stroke remains a leading contributor to the global disease burden.[4] In 2016, stroke was the second leading cause of death worldwide, claiming the lives of 5.5 million individuals. There are also an estimated 80 million survivors contending with stroke's deleterious effects.[5] The American Heart Association projects that by 2030, 4% of all adults will have experienced a stroke, and given the increasing aging global population, the number of total strokes is expected to double by 2050. The annual global cost related to stroke care in 2030 is estimated at $240.7 billion,[6] which is likely an underestimate given the contribution of stroke and cerebral ischemia to dementia and other comorbid conditions.[7] Furthermore, the social and emotional cost of stroke to patients, their loved ones, and caregivers is immense and unquantifiable.

Therapeutic perfusion with a recombinant tissue plasminogen activator (rtPA) and/or mechanical clot retrieval, thrombectomy, remains the only therapy for ischemic stroke.[8–11] However, the improvement rate for stroke patients using rtPA is relatively low due to several factors, including late hospital arrival, age of patients, and increased risk of intracerebral hemorrhage associated with delayed rtPA administration.[12,13] Thus, intensified efforts to mechanistically understand the pathophysiology of stroke and stem the tide of this disease are of the utmost importance.[14] Considering the ubiquity of this disease, identifying reversible risk factors or new therapeutic targets will have an outsized impact on the global disease burden. Both the central and systemic inflammatory responses are significantly implicated in the progression of stroke severity.[15] However, clinically efficacious immunomodulatory agents in addition to perfusion strategies (rtPA and/or thrombectomy) to critically attenuate induced pathogenic inflammation and fortify

[1]Department of Microbiology, Immunology & Molecular Genetics, University of Texas Health, San Antonio, TX, USA

[2]Division of Gastroenterology & Nutrition, Department of Medicine, University of Texas Health, San Antonio, TX, USA

[3]Department of Neurosciences, University of Florida, Gainesville, FL, USA

[4]Lead contact

*Correspondence: zadehm@uthscsa.edu

https://doi.org/10.1016/j.isci.2022.105437

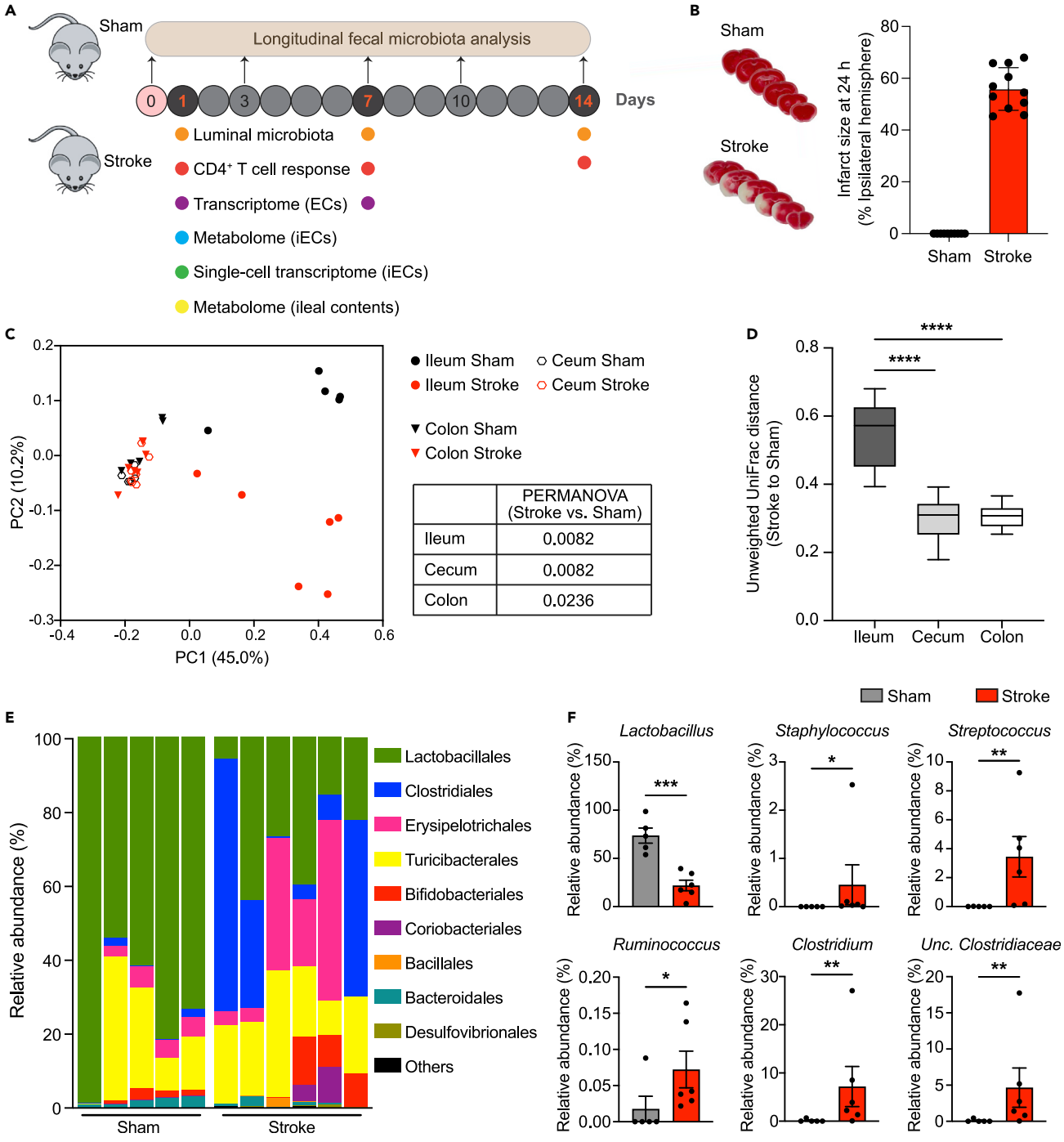

Figure 1. Ischemic stroke induces ileal microbiota changes

(A) Experimental scheme. Groups of C57BL/6 male mice (10–12 weeks old) were subjected to 45 min of transient middle cerebral artery occlusion (MCAO) or sham-operated to analyze the microbiome, epithelial cell (EC), and $CD4^+$ T-cell responses in the gut. Feces were collected from the 2 groups of mice on days 0 (baseline), 3, 7, 10, and 14 (after the surgery) for longitudinal microbiome analysis. The ileal, cecal, and colonic microbiomes and $CD4^+$ T cells were analyzed on days 1, 7, and 14 after stroke, and the bulk transcriptomes of ileal epithelial cells (iECs) were examined on days 1 and 7 after stroke. Single-cell RNA-seq profiling was conducted for iECs, and a metabolomic analysis was performed for iECs and ileal contents 1 day after stroke onset.

(B) Representative 2,3,5-triphenyltetrazolium chloride (TTC)-stained brain sections and graphical data showing the infarct sizes 1 day after the MCAO.

(C) Unweighted UniFrac principal coordinate analysis plot, obtained from 16S rRNA sequencing, depicts the bacterial community structures in the ileal, cecal, and colonic contents of poststroke and sham-operated mice 1 day after surgery (n = 5–6/group). Significance: PERMANOVA.

Figure 1. *Continued*

(D) Unweighted UniFrac distances between stroke and sham microbiome in the ileum, cecum, and colon. Significance: Mann-Whitney test.

(E) Top bacterial (order) abundance in the ileal contents of stroke and sham mice.

(F) The relative abundance of differential bacterial taxa at genus level. Significance: Mann-Whitney test. Bars indicate mean and SD. *, $p < 0.05$; **, $p < 0.01$; ***, $p < 0.001$; ****, $p < 0.0001$.

protective immune regulation are yet to be discovered.[16] Such a discovery may result in the significant reduction of perfusion injuries with a wider effective therapeutic window and the potential reach to a larger stroke-affected population.

Ample evidence now hints at the critical impact of intestinal homeostasis controlled by gut microbiota and the associated metabolites in regulating the local and central molecular response following stroke.[17–20] The accumulating evidence also suggests that stroke induces gut microbiota dysbiosis which exacerbates intestinal immune response, particularly interleukin (IL)-17$^+$ γδ T cells, resulting in enhanced neuroinflammation affecting poststroke recovery.[20–23] However, the intestinal epithelial cells (ECs), which not only sense microbiota-derived signals but also modulate host immune responses, are less well-understood in the context of ischemic stroke. Thus, to gain further critical insights into stroke-induced gene and metabolic events in the gut, we particularly focused on the involved molecular mechanisms potentially regulating the ileal epithelium, the gut microbiome, and associated metabolites in the host affected by induced ischemic stroke.

RESULTS

Ischemic Stroke Induces Gut Dysbiosis

Commensal gut microbiota plays a critical role in acute brain injury whereby gut dysbiosis, prior to ischemic stroke induction, affects disease pathogenesis.[23] To elucidate intestinal microbial and epithelial responses to stroke-induced brain injury, we employed multiomic approaches to comprehensively profile the impacts of ischemic stroke on gut microbiome, metabolome, transcriptome, and immune response (Figure 1A). We observed a clear and consistent brain infarct size in poststroke mice 1 day after 45 mins of transient middle cerebral artery occlusions (Figure 1B). To monitor stroke-induced microbial dynamics, we longitudinally analyzed the microbiome in the feces collected from poststroke mice and sham-operated controls of the same animals. During the acute phase of stroke, there was a trend toward a decrease in α-diversity in stroke mice (3 days after stroke induction), and this difference was reversed on day 14 (Figure S1A). An unweighted UniFrac principal coordinate analysis demonstrated that stroke significantly separated the fecal microbiomes from sham controls at any of the examined time points (Figure S1B), with a reduction in the Firmicutes/Bacteroidetes ratio on day 3 (Figure S1C), a typical feature of poststroke gut dysbiosis.[20,23] Further analysis revealed the gradual loss of *Turicibacter* and the enrichment of *Bacteroides ovatus* in the feces of poststroke mice (Figure S1D). The relative abundance of *Akkermansia muciniphila* and Ruminococcaceae was elevated during the acute phase of stroke, while members of Clostridia (Clostridiales, *Clostridium*, *Oscillospira*, and *Blautia*) were found at significantly higher levels in the poststroke mice than in sham controls during the chronic phase of stroke (Figure S1D).

To further explore the differences in microbial communities during the acute phase of stroke, we spatially examined the microbiota composition in the ileal, cecal, and colonic contents collected from poststroke and sham-operated mice 1 day following the surgery (Figure 1A). Data demonstrated that the ileal, cecal, and colonic microbiomes of poststroke mice significantly differed from those of sham controls, as determined by permutational multivariate analysis of variance (PERMANOVA) (Figure 1C). To assess the similarity between stroke and sham samples of the aforementioned regions, we calculated unweighted UniFrac distances, which were significantly higher in the ileum than those in the cecum and colon (Figure 1D), indicating that microbes residing in the ileum may be more responsive to acute ischemic stroke. Thus, further analyses were centered on the microbial responses in the ileal region. A compositional analysis revealed that ischemic stroke reduced the relative abundance of Lactobacillales (phylum Firmicutes) and Bacteroidales (phylum Bacteroidetes) in the ileal contents (Figure 1E). Consistently, the genus *Lactobacillus* was dramatically diminished in the stroke-affected group (20.4% on average) when compared to that in sham controls (65.1%) (Figure 1F). Additionally, potentially opportunistic pathogenic bacteria, including *Staphylococcus*, *Streptococcus*, and *Ruminococcus*, were rarely detected in the sham controls, but their levels

were significantly elevated following ischemic stroke. Consistent with a previous study,[21] *Clostridium* was also significantly increased in ileal contents of poststroke mice 1 day after stroke induction (Figure 1F).

Additionally, we analyzed the ileal, cecal, and colonic microbiome in the stroke and sham mice 7 and 14 days after stroke onset. Here, the microbial diversity was significantly reduced in the ileum and colon (Figure S2A), with a shift in the bacterial community structure, particularly in the ileum of poststroke mice on day 7 (Figure S2B). A similar pattern was observed 1 day after stroke induction (Figure 1A). Bacterial taxa, including *Bifidobacterium* (order Bifidobacteriales) and *Allobaculum* (order Erysipelotrichales), were completely depleted in the ileal contents of poststroke mice (Figures S2C and S2D). The relative abundance of Bacteroidales family S24-7 and *Adlercreutzia* also decreased significantly. Fourteen days after stroke, the α-diversity of the ileal microbiota still remained lower than that in sham controls (Figure S2E), and the abundance of S24-7 and *Allobaculum* was consistently reduced in stroke mice (Figure S2F). Intriguingly, levels of *Lactobacillus* were high in the ileum of poststroke mice (Figure S2F), in contrast with its reduced abundancy on day 1 (Figure 1D). These results indicate that ischemic stroke induces gut dysbiosis resulting in microbiome compositional changes associated with disease status.

Ischemic Stroke Affects Gut Microbiome-Associated Metabolites

To further evaluate the potential functional changes of gut microbiota due to ischemic stroke, we analyzed microbiota-associated metabolites in the ileal contents of mice 24 h after stroke onset and sham controls, which demonstrated distinct metabolomic profiles by both positive and negative ionizations (Figure 2A). Metabolic pathways related to amino acids (e.g., lysine, glycine, tyrosine, and tryptophan), carbohydrates (e.g., hexose, N-glycan, galactose, and sialic acid), vitamins (vitamin B6, vitamin C, and vitamin A), as well as propionate were all significantly impaired due to ischemic stroke (Figure 2B). Importantly, vitamin C (ascorbic acid and dehydroascorbate) and vitamin B6 (pyridoxine and pyridoxamine), critically supporting the growth of microbes, were reduced in the ileal contents of the stroke mice (Figure 2C). Metabolites exhibiting antioxidant properties (e.g., picolinic acid, quinate, shikimate, and 3-dehydroshikimate) and those associated with the tricarboxylic acid (TCA) cycle (e.g., citrate, isocitrate, and 2-hydroxyglutarate) were also reduced. Furthermore, decreased abundance of *Lactobacillus* (Figure 1F) correlated with declined levels of lactic acid in stroke mice (Figure 2C).

Certain dominant gut microbes, notably Bacteroidetes, possess a very large number of genes encoding carbohydrate-active enzymes.[24] Here, a reduced level of Bacteroidales (Figure 1E) was associated with declined capability of the ileal microbiota to metabolize carbohydrates in stroke mice, as revealed by the decreased availability of carbohydrates, including arabitol, sorbitol, psicose, and glucose/fructose (Figure 2C). However, the decreased availability of luminal carbohydrates may also be due to reduced food intake during the first day of stroke.[25] In contrast, most amino acids (e.g., aspartate, glycine, histidine, lysine, proline, and tryptophan) were abundant in the stroke group, which also demonstrated higher levels of chemicals that are indicative of inflammation-associated gut dysbiosis, such as formate[26] and trimethylamine N-oxide (TMAO), as a byproduct of microbial carnitine metabolism.[27]

Furthermore, trigonelline, oxfenicine, and ethanolamine may target peroxisome proliferator-activated receptors (PPARs) to inhibit cellular fatty acid oxidation (FAO).[28–30] Interestingly, these metabolites were all reduced in the ileal contents of poststroke mice compared to sham controls (Figure 2C). Furthermore, levels of azelaic acid, retinoic acid, and tauro-β-muricholic acid (TβMA), which has been reported to modulate PPAR activation,[31–33] were also differentially impacted, suggesting that induction of ischemic stroke leads to functional impairment of the ileal microbiota.

Ischemic Stroke Transcriptionally Activates Mitochondrial FAO and Metabolically Inhibits the TCA Cycle in Ileal Epithelial Cells

Having demonstrated the differential enrichment of microbiota-associated metabolites (Figure 2C), potentially impacting the host EC signaling,[34] we next elucidated the transcriptomic and metabolic responses of ileal epithelial cells (iECs) to acute ischemic stroke. An RNA sequencing analysis of iECs derived from the poststroke mice and sham controls demonstrated distinct global transcriptomes 1 day after the surgery (Figure 3A), resulting in 186 upregulated and 99 downregulated differentially expressed genes (DEGs) in the stroke-affected mice compared to sham controls (Figure 3B). Here, the top upregulated DEGs included 3-hydroxy-3-methylglutaryl-CoA synthase 2 (*Hmgcs2*) which is critical for ketogenesis,[35] long-chain acyl-CoA dehydrogenase (*Acadl*), acyl-CoA carboxylase beta (*Acacb*), acyl-CoA thioesterase 1 (*Acot1*), and carnitine/acylcarnitine translocase (*Slc25a20*) (Figures 3B and 3C), all of which are highly implicated in

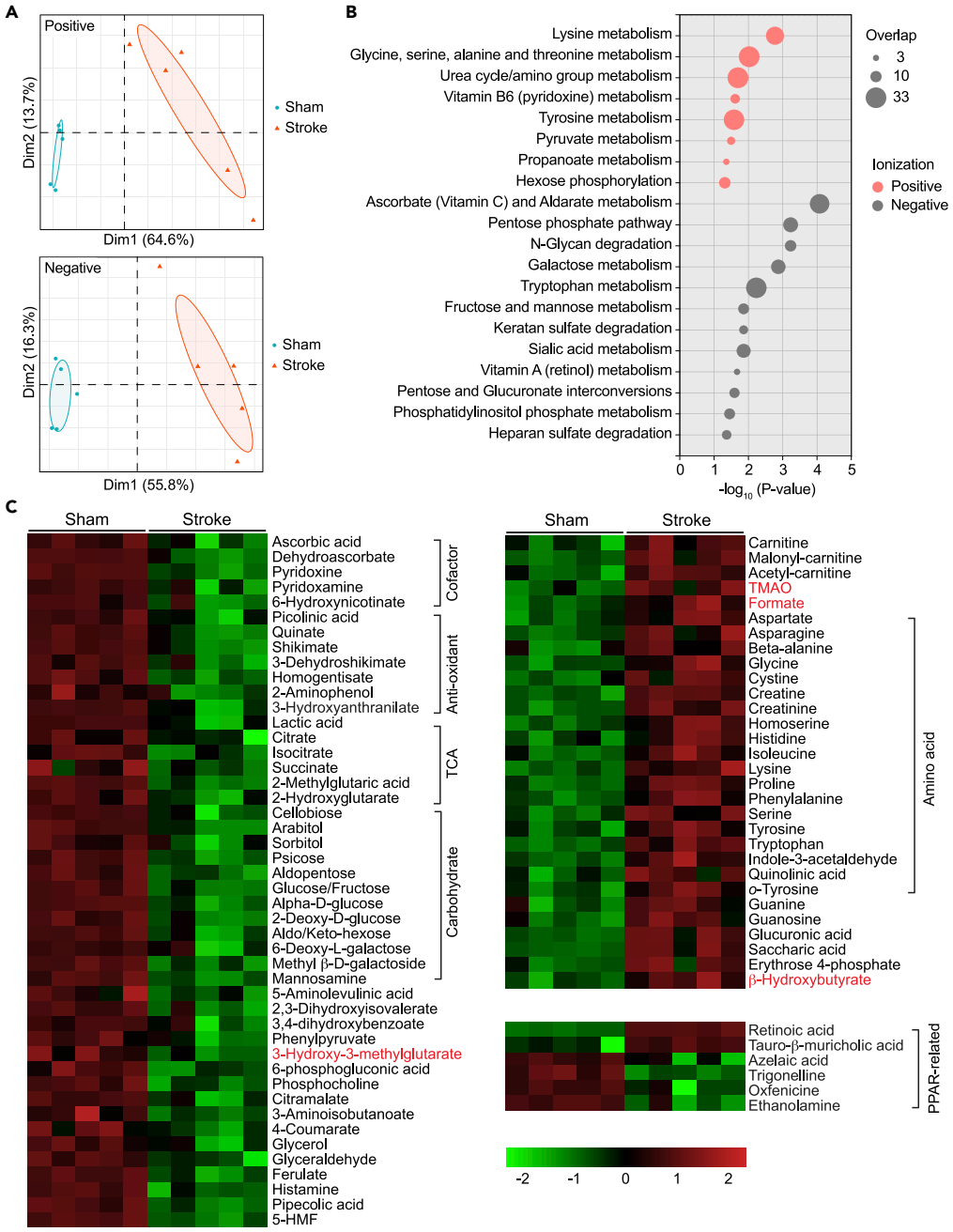

Figure 2. Ileal microbiota-associated metabolism is impaired due to ischemic stroke

(A) Principal component analysis (PCA) plots of metabolite features identified by positive and negative ionizations in ileal contents of poststroke and sham-operated mice 1 day after surgery (n = 5/group).

(B) Metabolic pathway analysis of metabolites with significantly differing intensity between stroke and sham mice. The overlapped size indicates the number of significant metabolic features mapped to corresponding pathways.

(C) Heatmap showing differentially enriched metabolites.

mitochondrial FAO. A gene set enrichment analysis (GSEA) further demonstrated that FAO and the fatty acid metabolic process were the major pathways enriched in iECs of stroke mice (Figure 3D). Accordingly, a set of FAO-associated mitochondrial genes (e.g., *Hmgcs2*, *Acaa2*, *Acadl*, *Hadha*, and *Hadhb*), cytochrome P450 enzymes (*Cyp2* and *Cyp4* families) involved in cytoplasmic fatty acid metabolism, and genes (*Fabp1* and *Apoc2*) related to intracellular lipid transport and trafficking were all activated in iECs by

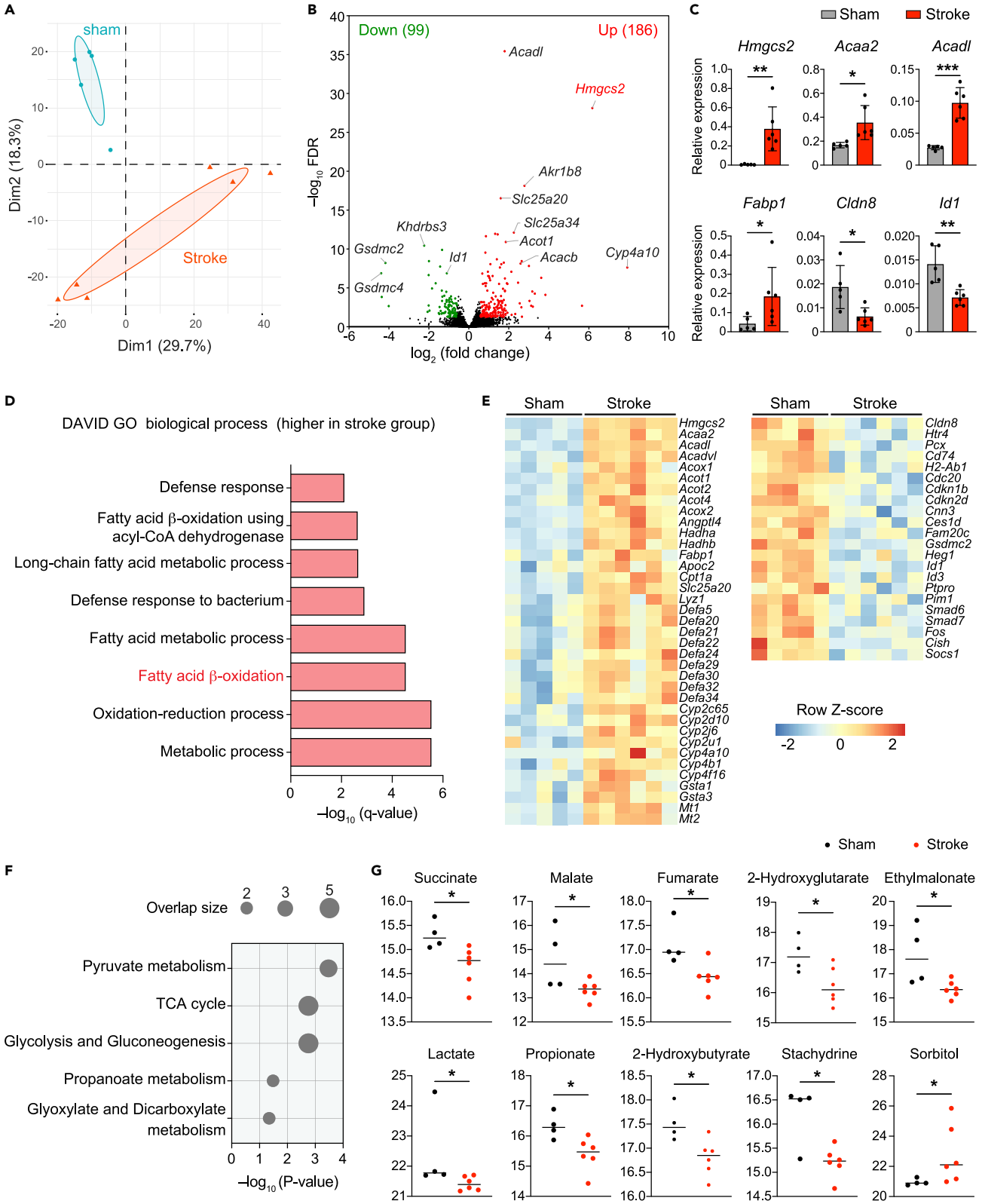
A
sham
Stroke
Dim2 (18.3%)
Dim1 (29.7%)
B
Down (99)
Up (186)
Acadl
Hmgcs2
Akr1b8
Slc25a20
Slc25a34
Acot1
Acacb
Cyp4a10
Khdrbs3
Gsdmc2
Id1
Gsdmc4
−log10 FDR
log2 (fold change)
C
Sham
Stroke
Hmgcs2
Acaa2
Acadl
Fabp1
Cldn8
Id1
Relative expression
D
DAVID GO biological process (higher in stroke group)
Defense response
Fatty acid β-oxidation using acyl-CoA dehydrogenase
Long-chain fatty acid metabolic process
Defense response to bacterium
Fatty acid metabolic process
Fatty acid β-oxidation
Oxidation-reduction process
Metabolic process
−log10 (q-value)
E
Sham
Stroke
Hmgcs2
Acaa2
Acadl
Acadvl
Acox1
Acot1
Acot2
Acot4
Acox2
Angptl4
Hadha
Hadhb
Fabp1
Apoc2
Cpt1a
Slc25a20
Lyz1
Defa5
Defa20
Defa21
Defa22
Defa24
Defa29
Defa30
Defa32
Defa34
Cyp2c65
Cyp2d10
Cyp2j6
Cyp2u1
Cyp4a10
Cyp4b1
Cyp4f16
Gsta1
Gsta3
Mt1
Mt2
Cldn8
Htr4
Pcx
Cd74
H2-Ab1
Cdc20
Cdkn1b
Cdkn2d
Cnn3
Ces1d
Fam20c
Gsdmc2
Heg1
Id1
Id3
Ptpro
Pim1
Smad6
Smad7
Fos
Cish
Socs1
Row Z-score
F
Overlap size
Pyruvate metabolism
TCA cycle
Glycolysis and Gluconeogenesis
Propanoate metabolism
Glyoxylate and Dicarboxylate metabolism
−log10 (P-value)
G
Sham
Stroke
Succinate
Malate
Fumarate
2-Hydroxyglutarate
Ethylmalonate
Lactate
Propionate
2-Hydroxybutyrate
Stachydrine
Sorbitol

Figure 3. Stroke enhances FAO and reduces TCA cycle in iECs

(A) PCA plot of iEC transcriptomes between stroke and sham-treated mice 1 day after stroke onset (n = 5–6/group).

(B) Volcano plot of DEGs between the 2 groups of iECs. The number of upregulated and downregulated DEGs in stroke group is indicated in parentheses.

(C) qRT-PCR validation of representative DEGs.

(D) Significantly enriched pathways in the stroke group, obtained from DAVID gene ontology (GO) database, related to the biological process. Note: no significant pathways were identified using downregulated DEGs.

(E) Heat maps of representative DEGs obtained from RNA sequencing results.

(F) Significant metabolic pathways of iECs isolated from mice 1 day after stroke or sham treatment (n = 5/group). The overlapped size indicates the number of significant metabolic features mapped to the indicated pathways.

(G) Scatter plots of metabolites differentially enriched in iECs of stroke and sham mice. Bars indicate mean and SD. *, $p < 0.05$; **, $p < 0.01$; ***, $p < 0.001$; two-tailed unpaired t test (C and G).

ischemic stroke (Figure 3E). These cells also had enhanced expression of antimicrobial alpha-defensins (e.g., *Defa5*, *Defa21*, *Defa29*, and *Defa34*) and lysozyme (*Lyz1*) in addition to enriched transcripts associated with antioxidant defense responses (*Gsta1* and *Gsta3*). Metallothioneins (*Mt1* and *Mt2*), known to be highly induced in the mouse brain during the early phase of ischemic stroke,[36] were also stimulated in iECs 1 day after stroke induction. Additionally, stroke suppressed the expression of genes related to barrier integrity (*Cldn8*), neuronal signaling (*Htr4*), antigen processing and presentation (*Cd74* and *H2-Ab1*), and EC differentiation (e.g., *Cdkn1b*, *Id1*, and *Id3*), as well as transcripts negatively regulating inflammatory responses (*Cish* and *Socs1*) (Figure 3E).

Importantly, an untargeted cellular metabolomic analysis of iECs isolated from ischemic stroke and sham control mice 1 day after the surgery demonstrated impaired pathways related to pyruvate metabolism and the TCA cycle (Figure 3F). Specifically, levels of TCA cycle intermediates, including succinate, malate, fumarate, and 2-hydroxyglutarate,[37] were evidently decreased in iECs derived from poststroke mice (Figure 3G). Lactate and propionate, promoting intestinal epithelial turnover,[38,39] were also reduced in these cells. Additionally, 2-hydroxybutyrate, associated with propionate metabolism, was also decreased. Furthermore, stachydrine, exerting neuroprotective properties,[40] was diminished, while sorbitol contributing to oxidative stress[41] was augmented in iECs of poststroke mice. These results thus indicate that induced ischemic stroke disrupts the mitochondrial metabolic homeostasis in iECs.

To elaborate on regionally specific responses of ECs to ischemic stroke, we spatially analyzed and compared the transcriptomes of cecal and colonic ECs and iECs. Obtained results revealed that not only iECs (Figure 3A) but also cecal and colonic ECs (Figure S3A) exhibited unique transcriptomic profiles 1 day after ischemic stroke. A differential expression analysis showed that genes associated with fatty acid metabolism, as top DEGs, were elevated in cecal (*Pdk4*, *Acot1*, and *Acot2*) and colonic ECs (*Cyp2d12*, *Cyp2d34*, *Acot1*, *Acot2*, and *Acadl*) (Figure S3B). The cecal ECs of stroke mice were primarily enriched with transcripts involved in the host defense response, potentially as a result of gut dysbiosis, whereas activities of cholesterol and steroid metabolic processes were decreased (Figure S3C). In the colon, cell cycle and cell division were the major pathways that were suppressed by stroke. Interestingly, comparisons of cecal and colonic ECs with iECs identified 15 upregulated and 6 downregulated DEGs (Figure S3D) in the stroke group, regardless of anatomic locations. A search tool for recurring instances of neighboring genes (STRING) analysis depicted a major interactive network of upregulated DEGs, which can be activated by PPARs (except *Eci2*) and are highly associated with FAO (Figure S3D).

To further define the stroke-responsive epithelial gene signatures, we analyzed the transcriptomes of iECs isolated from poststroke mice and sham-operated controls 7 days after the surgery. Here, ischemic stroke induction also resulted in global transcriptional separation (Figure S4A), with top upregulated DEGs primarily associated with the lipid metabolic activity (e.g., *Scd1*, *Apob*, and *Acaa1b*) (Figure S4B). To identify iEC-enriched gene signatures, we compared the DEGs enriched on day 7 with DEGs characterized on day 1 after stroke (Figure S4C). The genes with a conserved iEC expression included *Hmgcs2* and *Acox2*, which are involved in PPAR signaling and FAO, as well as transcripts related to pyroptosis (*Gsdmc2*, *Gsdmc3*, and *Gsdmc4*) and epithelium development (*Hbegf* and *Serpinb5*) (Figure S4D).

Single-Cell RNA Sequencing Reveal Cell Subset-Specific Signatures of iECs Affected by Ischemic Stroke

Knowing that intestinal epithelial FAO is critical for regulating the differentiation and maintenance of intestinal stem and progenitor cells,[42,43] its dysregulation due to ischemic stroke may impact the epithelial structure and

function. Given that the FAO pathway was more pronounced in iECs of poststroke mice on day 1 (Figure 3D) than in cecal or colonic ECs (Figure S3) or iECs derived from poststroke mice on day 7 (Figure S4), we performed an single-cell RNA sequencing analysis of iECs isolated from poststroke mice and sham controls 1 day after surgery to gain further insights into gene transcripts in different iEC subpopulations. After quality filtering, the transcriptomic profiles of 38,234 iECs were collected (21,565 cells from 3 stroke mice and 16,669 from 3 sham control mice). Cells were sequenced to comparable sequencing depths (~44,000–64,000 reads/cell) and had similar median genes per cell (~3,000–4,000 genes/cell). To identify transcriptional differences in iEC subsets, we performed dimensionality reduction and clustering, whereupon 14 groups were visualized by uniform manifold approximation and projection and labeled by the expression of known marker genes (Figures 4A and S5A). The stem, enteroendocrine (EEC), Paneth, and tuft cells were each represented by a single distinct cluster, while transit-amplifying (TA), goblet, and absorptive enterocytes were partitioned across several clusters representing different stages of cell maturation (Figure 4A).

To analyze the impact of stroke on shifts in cell composition, the frequencies of each cell subset in each sample were calculated, as defined by unsupervised clustering (Figure 4A). Induced ischemic stroke substantially decreased the frequency of goblet cells (from 10.7% on average in sham to 3.9% in stroke) and significantly reduced the proportion of tuft cells (3.5% to 2.3%) (Figure 4B). A gene expression analysis showed that a set of genes encoding alpha-defensins (e.g., *Defa5 and Defa21*), normally expressed by Paneth cells, were induced in all cell types by stroke, while genes related to antigen processing and presentation (e.g., *Cd74 and H2-Aa*) were markedly reduced, particularly in mature enterocytes (Figure S5B). Notably, *Hmgcs2* was expressed at very low levels in highly proliferating cells of the sham control mice; however, its expression was dramatically increased in iECs, particularly in stem and TA cells derived from mice affected by stroke (Figure 4C). These cell subsets were also enriched with transcripts related to FAO, including *Acadl* and *Fabp1* (Figure S5C). Additionally, the stress-induced RNA-binding motif protein 3 (*Rbm3*) exhibiting a neuroprotective function after an hypoxic-ischemic brain injury[44] and antimicrobial peptide *Reg3b*, which is normally enterocyte-specific, were both activated in all the cell types by stroke (Figure 4C).

Furthermore, cell-type-specific responses were identified. Here, ischemic stroke stimulated mature enterocytes with increased expression of genes associated with lipid metabolism (e.g., *Apoa4*, *ApoC2*, and *Fabp2*) and the calcium-binding protein (*S100a6*) (Figure 4D), which can be activated by stress conditions, including ischemia.[45] In EECs, ischemic stroke suppressed the expression of *Neurog3*, *Sox4*, and *Insm1*, controlling EEC differentiation and development, and enhanced the expression of peptide YY (*Pyy*), potentially negatively regulating appetite and food intake.[46,47] Interestingly, we also observed the suppression of genes critically involved in mucin production (*Mus2* and *Agr2*) by goblet progenitors, as well as transcripts crucially promoting cell proliferation (*Mki67* and *Top2a*) (Figure 4D), potentially accounting for the reduced numbers of goblet cells in stroke mice (Figure 4B). Furthermore, stroke not only decreased the number of tuft cells (Figure 4B) but also may functionally reduce the tuft cell activity, as demonstrated by diminished transcripts of *Trpm5*, *Nrep*, *Plcb*, and *Plcg* (Figure 4D).

Finally, DAVID gene ontology analysis using differentially enriched genes in each cell subsets further demonstrated that pathways involved in the defense response to a bacterium were activated in secretory cell subsets, including goblet, tuft, and EEC cells by stroke, due to increased production of antimicrobial peptides. Stroke also reduced the activity of antigen processing and presentation in enterocytes and stem cells and inhibited the endocrine pathway in EECs (Figure S5D). These results suggest that ischemic stroke fundamentally and functionally impacts the molecular machinery of iECs in a cell-subset-specific manner.

Ischemic Stroke Affects Ileal IL-17A$^+$ γδ T and CD4$^+$ T-cell Responses

Gut microbiota and intestinal ECs are highly involved in the regulation of gut immune homeostasis.[48–50] Having shown that ischemic stroke induced gut dysbiosis and functionally affected iECs, including a reduction of antigen processing and presentation, we then addressed whether the intestinal T-cell response was also altered in mice after stroke induction. Flow cytometric analysis of ileal, cecal, and colonic T cells demonstrated that CD4$^+$ T-cell numbers were substantially decreased in the ileum but not in cecum or colon 7 days after stroke onset (Figure 5A). Consistent with a previous report,[23] we also observed a significant increase in both the frequency and number of ileal IL-17A$^+$ γδ T cells in ischemic stroke-affected mice, while stroke impacted cecal and colonic IL-17A$^+$ γδ T cells to a lesser extent (Figure 5B). Dysfunctional CD4$^+$ T cells, particularly regulatory T cells (Tregs), have been implicated in mechanisms of stroke-induced inflammation and tissue injury.[51,52] Here, the frequency and number of IL-10$^+$ Tregs were significantly

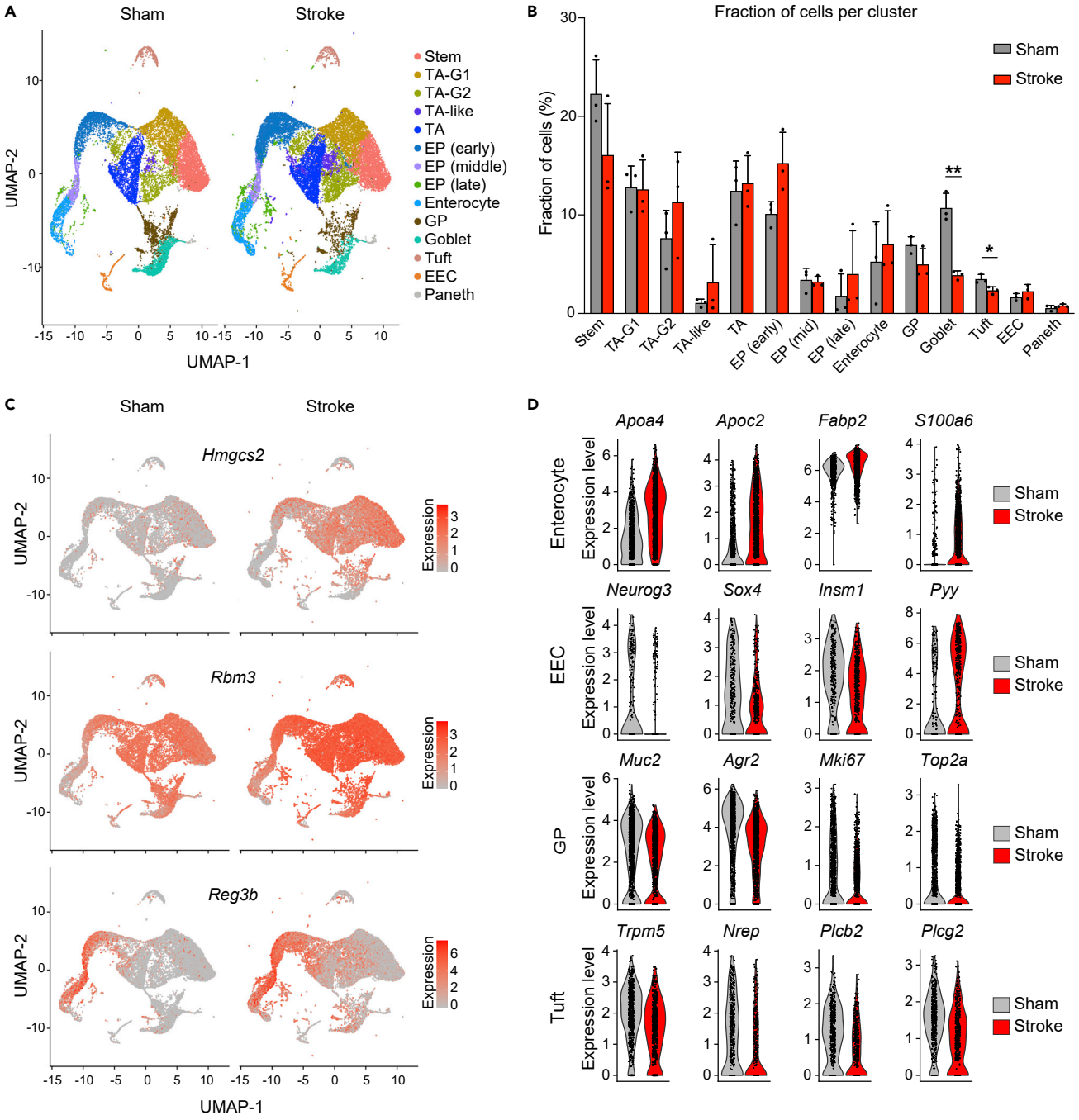

Figure 4. Single-cell RNA sequencing reveals cell-subset-specific changes induced by ischemic stroke

(A) Cell-type clusters split by conditions (stroke and sham). We used uniform manifold approximation and projection (UMAP) to visualize the clustering (color coding) of 21,565 single cells isolated from 3 stroke mice and 16,669 single cells isolated from 3 sham mice, based on the expression of known markers. TA, transit-amplifying; G1 and G2, cell-cycle phase; EP, enterocyte progenitor; GP, goblet progenitor; EEC, enteroendocrine.

(B) The proportion of each cell type in the ileum. Bars indicate mean and SD. *, $p < 0.05$; **, $p < 0.01$; two-tailed unpaired t test.

(C) Feature plots showing the expression profile of *Hmgcs2*, *Rbm3*, and *Reg3b* genes in sham-operated and poststroke mice 1 day after stroke induction.

(D) Violin plots of representative DEGs in indicated cell types between the stroke and sham groups. For all the comparisons, false discovery rate < 5.56e-06.

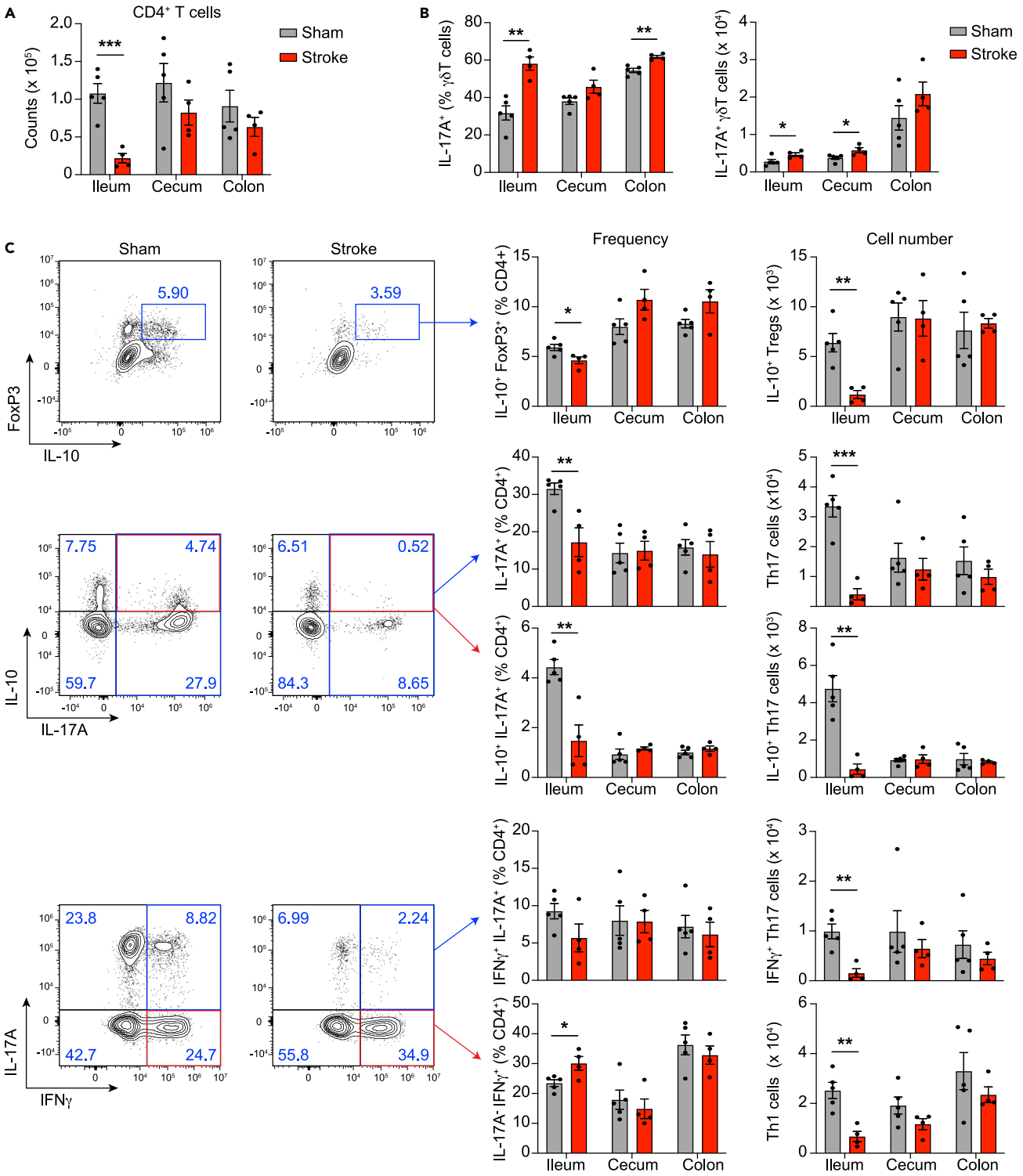

Figure 5. Stroke increases IL-17A-producing γδ T cells and inhibits CD4$^+$ T-cell responses in the ileum

(A) The total number of CD4$^+$ T cells in the ileum, cecum, and colon 7 days after stroke and sham treatment (n = 5/group). One mouse succumbed to ischemic stroke before the experiment was terminated on day 7.

(B) The frequencies and counts of IL-17A$^+$ γδ T cells in the indicated intestinal regions.

(C) The representative flow plots, frequencies, and counts of IL-10$^+$ FoxP3$^+$ Tregs, IL-10$^+$ Th17, IFNγ$^+$ Th17, and Th1 cells in the ileum, cecum, and colon. Data are representative of 2 independent experiments. Bars indicate mean and SEM. *, $p < 0.05$; **, $p < 0.01$; ***, $p < 0.001$; two-tailed unpaired t test.

reduced in the ileum, but not in the cecum or colon after stroke (Figure 5C). The frequency of Th17 cells, and particularly those producing IL-10, possessing a regulatory function,[50] was also significantly diminished in the ileum of poststroke mice, while the percentage of IFN-γ^+ Th17 cells remained unchanged. Reduced immune regulation in the ileum of stroke mice may result in increased IL-17A$^-$ IFNγ^+ Th1 cells. Due to decreases in CD4$^+$ T cells, the numbers of all the examined CD4$^+$ T cell subsets were reduced in the ileum by stroke. In the cecum or colon, neither the frequencies nor the numbers of CD4$^+$ T cells significantly differed (Figure 5C), suggesting that induced ischemic stroke dampens the CD4$^+$ T-cell immune responses specifically in the ileum wherein microbial and epithelial functions were highly influenced.

Within 1 day of ischemic stroke, the frequency and number of IL-10$^+$ Tregs and Th1 cells were also reduced in the ileum of poststroke mice, while there was no difference in CD4$^+$ T-cell number or Th17 cells (Figure S6A), both of which were dramatically decreased on poststroke day 7 (Figures 5A and 5C). Fourteen days after stroke onset, the poststroke mice exhibited a similar immunological phenotype as those of poststroke day 7, including the reductions of CD4$^+$ T cells, IL-10$^+$ Tregs, and Th17 cells, and augmentation of IL-17A$^+$ $\gamma\delta$ T cells in the ileum (Figure S6B), potentially indicating an evolving and persistent impact of cerebral ischemic stroke on the intestinal immune response.

DISCUSSION

The complex interplay with the intestinal epithelium, microbiome, associated metabolites, and immunological cascades contributes to the maintenance of host intestinal homeostasis.[53] Disruption of such a functional homeostatic condition (termed gut dysbiosis) has been implicated in the pathogenesis and development of not only intestinal but also neurological diseases, including Parkinson's disease and Alzheimer's disease.[54] Recent studies also revealed that gut microbiota influences the neuropathology and outcomes of ischemic stroke,[23] whereupon induced gut dysbiosis critically impairs the gut-cerebral signaling, resulting in intestinal barrier dysfunction, endotoxemia, and toxic systemic inflammation, all of which profoundly affect the poststroke outcomes.[55] Yet, the molecular and metabolic mechanisms implicated in ravaging iECs and exacerbating the ischemic stroke disease progression are still elusive. Thus, in the present study, we comprehensively elucidated the impact of induced ischemic stroke on the gut microbiota and their associated metabolites, and iECs, as well as the immune responses. Our results demonstrated that while stroke critically altered the gut microbial composition and associated metabolisms, these signals, in tandem, differentially impacted distinct subsets within iECs and fundamentally modified the EC structure and function.

Numerous studies have reported that stroke induces gut microbial changes in mice that exacerbate the disease outcomes through immune-mediated mechanisms.[20,22,23,56] In this scenario, antibiotic-treated mice have reduced pathogenic IL-17$^+$ $\gamma\delta$ T cells that can traffic to the brain to enhance ischemic neuroinflammation. The changes in IL-17$^+$ $\gamma\delta$ T cells are solely observed in the small intestine, but not in the colon or systemic sites such as spleen.[23] Here, we consistently demonstrated that induced ischemic stroke orchestrated a more pronounced impact on the microbial composition and IL-17$^+$ $\gamma\delta$ T cells in the ileum than on those in the cecum or colon. This may be due to inherent anatomical differences in neuron innervation and blood supply.[57,58] Accordingly, compared to the lower gastrointestinal (GI) tract, the small intestine is richly supplied with efferent vagal nerves.[59] The vascular supply is also greater in the proximal intestine than in the distal intestine.[60] Furthermore, the upper GI hemorrhage is more common in patients with acute ischemic stroke.[61] Thus, ileal region may be a primary target of stroke.

Our observations involving ileal microbiota changes were in line with previous findings showing reduced abundance of *Lactobacillus* in monkeys with cerebral ischemia[62] and enriched *Ruminococcus* in patients with stroke.[63] More importantly, we further demonstrated that the microbiota-associated metabolic function was significantly affected by ischemic stroke. Here, stroke not only impaired the capabilities of the gut microbiota to metabolize carbohydrates but also reduced the levels of antioxidant chemicals and increased inflammatory signals in the ileal lumen. It is reported that gut microbiota metabolizes dietary carnitine to generate TMAO,[64] a potential causative factor in various cardiovascular diseases and ischemic stroke.[27] Both carnitine and TMAO were found at significantly higher levels in stroke mice than in sham controls. Additionally, studies also document that formate is solely produced by gut microbes, and its level can be highly elevated by gut dysbiosis-induced inflammation, whereby it may serve as an electron donor to favor the outgrowth of Enterobacteriaceae.[26] Here, we also found that ileal contents associated with stroke-induced gut dysbiosis were highly enriched with formate, consistent with a previous report demonstrating the elevated level of formate in the plasma of stroke patients.[65]

Many gut microbiota-derived metabolic products serve as signaling factors and engage various gene and metabolic networks in the host cells, including iECs.[66] We demonstrated that ischemic stroke diminished the levels of fecal metabolites, including trigonelline, oxfenicine, and ethanolamine, potentially inhibiting the cellular FAO.[28–30] Analyzing the transcriptomes of iECs further supported the notion that mitochondrial FAO was enhanced during the acute phase of stroke, while the TCA cycle was diminished, as documented by the cellular metabolomic analysis. Such an outcome potentially indicates that instead of fueling the TCA cycle, acetyl-CoA generated by mitochondrial FAO may be skewed toward ketogenesis through β-hydroxy-β-methylglutaryl-CoA.[67] This hypothesis is supported by the fact that ischemic stroke dramatically increased the expression of *Hmgcs2* in iECs, the gene encoding the rate-limiting enzyme in the production of ketone bodies.[35,68] Although we did not detect metabolites of ketogenic pathway in iECs, possibly due to limited cell numbers and assay sensitivity, these metabolites, particularly β-hydroxybutyrate, could easily diffuse across the cell membrane to be detected in the ileal contents (Figure 2C). β-Hydroxybutyrate inhibits the histone deacetylase activity in intestinal stem cells to enhance Notch signaling.[69] Thus, loss of *Hmgcs2* depletes the cellular levels of β-hydroxybutyrate, skewing stem cell differentiation toward secretory cell fates, including goblet cells.[69] Consistent with these results, we found that the elevated expression of *Hmgcs2* was associated with a reduced frequency of goblet cells.

HMGCS2 has been shown to interact with PPARα/γ and act as a coactivator to stimulate the transcription from the peroxisome proliferator response element of its own gene.[70,71] Accordingly, trigonelline, downregulating PPARγ expression in adipocytes,[28] and oxfenicine, an inhibitor of carnitine palmitoyltransferase 1B, were both decreased in the luminal contents of poststroke mice, while retinoic acid, an agonist of retinoid X receptor binding to PPARγ to coactivate downstream gene expression,[32] was enhanced. Moreover, levels of azelaic acid and TβMA, implicated in the modulation of PPAR activation,[31,33] were also impacted by stroke. Additionally, iECs were enriched with a set of genes, including *Hmgcs2*, *Acox1*, *Acot1*, *Cpt1a*, *Fabp1*, and *Angptl4*, which can be activated by PPARα and/or PPARγ, after stroke. Together, these results raise the possibility that stroke-induced gut dysbiosis critically affected gut microbial composition and metabolism to generate metabolic signals that may activate FAO and *Hmgcs2* in iECs through PPAR stimulation. In the cecum and colon, we also detected the activation of FAO-associated genes (e.g., *Acadl* and *Eci2*) in stroke mice, but the number of genes and the extent of activation, as determined by GSEA, were less than those in the ileum. In contrast to marked activation in iECs, *Hmgcs2* expression was unaffected in the cecal and colonic ECs after stroke, highlighting a region-specific impact of stroke on ECs. The activation of *Hmgcs2* in iECs may direct the mitochondrial FAO from the TCA cycle toward ketogenesis, potentially leading to the impairment of stem cell differentiation into mature goblet cells. Furthermore, studies show that microbiota-derived succinate promotes goblet and tuft cell hyperplasia through binding to its receptor SUCNR1.[72] Here, we observed reduced levels of succinate in the ileal lumen of stroke mice, which might also contribute to decreases in goblet and tuft cells.

Goblet cells synthesize mucin glycoproteins, such as MUC2 that are crucial for maintaining the intestinal barrier integrity by separating gut microbiota from the epithelium.[73] Stroke reduced the frequency of goblet cells and impaired the expression of *Muc2* in the ileum, which may contribute to increased intestinal permeability, resulting in bacterial translocation and systemic infection, a common consequence of ischemic stroke.[74] Tuft cells are the chemosensory sentinels of the gut and are enriched with taste-sensing molecules, including *Trpm5*,[75] while EECs secrete gut hormones (e.g., PYY) that control intestinal motility and absorption and regulate appetite.[76] Thus, the impairment of tuft and EECs may result in dysregulation of appetite and satiety, affecting nutritional intake in patients with ischemic stroke,[77] which may further exacerbate toxic inflammation in the hosts due to deficiency in micronutrients.

It is well-documented that gut microbial gene products can be sampled by intestinal ECs to potentially induce an antigen-specific T-cell response (e.g., Th17 cells) in the small intestine.[78] Here, stroke almost depleted mature enterocytes with transcripts involved in antigen processing and presentation, which correlated with reduced numbers of $CD4^+$ T cells in stroke mice compared to those in sham controls. In accordance with previous results that IL-17^+ γδ T cells can migrate to the brain and aggravate the ischemic stroke injury,[23] we also observed increased numbers and frequencies of these cells in the ileal region. Although intestinal Tregs do not enter the brain in the acute phase of stroke,[79] these cells are critical for maintaining intestinal homeostasis by restricting the differentiation of γδ T cells[80] and Th1 cells.[81] Thus, the reduction of IL-10^+ Tregs and IL-10^+ Th17 cells, associated with dysbiotic gut microbiota, may further exacerbate the inflammatory responses in the gut, as seen by increased IL-17^+ γδ T cells and disturbed Th1/Treg balance.

In summary, our results correlatively demonstrated that acute ischemic stroke induced gut dysbiosis and impaired microbial metabolic function, potentially reprogramming the cellular gene and metabolic signaling in iECs to influence EC structure and function. Thus, these deep insights into the cellular and molecular machinery of iECs may provide alternative targets to potentially design therapeutic interventions for the treatment of ischemic stroke.

Limitations of the Study

Although we have demonstrated the critical impact of ischemic stroke on gut microbiome, epithelial and immune responses, additional studies are still necessary to mechanistically interrogate the causative relationship between these complex interplays. Furthermore, although our data conspicuously demonstrated the transcriptional activation of *Hmgcs2* in iECs by ischemic stroke, its functional implication in potentially altering protein enzymatic activities still requires further elucidation. Thus, future research examining the critical role of genes, particularly *Hmgcs2*, during induced ischemic stroke may advance the development of gene targets for disease treatment. Additionally, only 10- to 12-week-old male mice were used in this study; thus, it remains to be determined whether the observations depend on sex- and age-related factors. Furthermore, a comprehensive study may be of critical interest to fully illuminate the impact of ischemic stroke on the human microbiome and associated metabolites, particularly the molecular and metabolic events in iECs of human stroke patients.

STAR★METHODS

Detailed methods are provided in the online version of this paper and include the following:

- KEY RESOURCES TABLE
- RESOURCE AVAILABILITY
  - Lead contact
  - Materials availability
  - Data and code availability
- EXPERIMENTAL MODEL AND SUBJECT DETAILS
  - Animals
- METHOD DETAILS
  - Transient middle cerebral artery occlusion (MCAO) model
  - Gut microbiota analysis
  - Metabolomic analysis
  - Isolation of epithelial cells (ECs)
  - Bulk RNA-seq
  - Single-cell RNA-seq
  - qRT-PCR
  - Flow cytometry
- QUANTIFICATION AND STATISTICAL ANALYSIS

SUPPLEMENTAL INFORMATION

Supplemental information can be found online at https://doi.org/10.1016/j.isci.2022.105437.

ACKNOWLEDGMENTS

This research was supported by NIH R01 DK109560, NIH R01 DK109560C, and NIH R01AI154630-01 to M.M.

AUTHOR CONTRIBUTIONS

M.M. directed the cellular and molecular studies and supervised data analyses. Y.G. performed cellular and molecular studies and bioinformatically analyzed the data. Y.G., M.Z., C.Y., and E.C.-J. performed and supervised animal experiments. Y.G. and M.M. interpreted the data and wrote the manuscript. All the authors received the manuscript to review and offer comments before its submission to the journal.

DECLARATION OF INTERESTS

The authors declare no competing interests.

Received: May 13, 2022
Revised: September 13, 2022
Accepted: October 19, 2022
Published: November 18, 2022

REFERENCES

1. Kinlay, S. (2011). Changes in stroke epidemiology, prevention, and treatment. Circulation *124*, e494–e496.

2. Kuklina, E.V., Tong, X., George, M.G., and Bansil, P. (2012). Epidemiology and prevention of stroke: a worldwide perspective. Expert Rev. Neurother. *12*, 199–208.

3. Hankey, G.J. (2014). Secondary stroke prevention. Lancet Neurol. *13*, 178–194.

4. Sevick, L.K., Ghali, S., Hill, M.D., Danthurebandara, V., Lorenzetti, D.L., Noseworthy, T., Spackman, E., and Clement, F. (2017). Systematic review of the cost and cost-effectiveness of rapid endovascular therapy for acute ischemic stroke. Stroke *48*, 2519–2526.

5. Gorelick, P.B. (2019). The global burden of stroke: persistent and disabling. Lancet Neurol. *18*, 417–418. https://doi.org/10.1016/S1474-4422(19)30030-4.

6. Ovbiagele, B., Goldstein, L.B., Higashida, R.T., Howard, V.J., Johnston, S.C., Khavjou, O.A., Lackland, D.T., Lichtman, J.H., Mohl, S., Sacco, R.L., et al. (2013). Forecasting the future of stroke in the United States: a policy statement from the American Heart association and American stroke association. Stroke *44*, 2361–2375.

7. Vermeer, S.E., Longstreth, W.T., Jr., and Koudstaal, P.J. (2007). Silent brain infarcts: a systematic review. Lancet Neurol. *6*, 611–619.

8. Nogueira, R.G., and Ribó, M. (2019). Endovascular treatment of acute stroke. Stroke *50*, 2612–2618. https://doi.org/10.1161/STROKEAHA.119.023811.

9. Furlan, A.J. (2015). Endovascular therapy for stroke–it's about time. N. Engl. J. Med. *372*, 2347–2349. https://doi.org/10.1056/NEJMe1503217.

10. Caplan, L.R., Furlan, A.J., and Hacke, W. (2015). Acute ischemic stroke therapy: the way forward. JAMA Neurol. *72*, 1405–1406. https://doi.org/10.1001/jamaneurol.2015.2872.

11. Campbell, B.C.V., Mitchell, P.J., Kleinig, T.J., Dewey, H.M., Churilov, L., Yassi, N., Yan, B., Dowling, R.J., Parsons, M.W., Oxley, T.J., et al. (2015). Endovascular therapy for ischemic stroke with perfusion-imaging selection. N. Engl. J. Med. *372*, 1009–1018. https://doi.org/10.1056/NEJMoa1414792.

12. Dávalos, A., Cobo, E., Molina, C.A., Chamorro, A., de Miquel, M.A., Román, L.S., Serena, J., López-Cancio, E., Ribó, M., Millán, M., et al. (2017). Safety and efficacy of thrombectomy in acute ischaemic stroke (REVASCAT): 1-year follow-up of a randomised open-label trial. Lancet Neurol. *16*, 369–376. https://doi.org/10.1016/S1474-4422(17)30047-9.

13. Miller, D.J., Simpson, J.R., and Silver, B. (2011). Safety of thrombolysis in acute ischemic stroke: a review of complications, risk factors, and newer technologies. Neurohospitalist *1*, 138–147. https://doi.org/10.1177/1941875211408731.

14. Kuriakose, D., and Xiao, Z. (2020). Pathophysiology and treatment of stroke: present status and future perspectives. Int. J. Mol. Sci. *21*, E7609. https://doi.org/10.3390/ijms21207609.

15. Jayaraj, R.L., Azimullah, S., Beiram, R., Jalal, F.Y., and Rosenberg, G.A. (2019). Neuroinflammation: friend and foe for ischemic stroke. J. Neuroinflammation *16*, 142–224.

16. Lakhan, S.E., Kirchgessner, A., and Hofer, M. (2009). Inflammatory mechanisms in ischemic stroke: therapeutic approaches. J. Transl. Med. *7*, 97.

17. Yamashiro, K., Kurita, N., Urabe, T., and Hattori, N. (2021). Role of the gut microbiota in stroke pathogenesis and potential therapeutic implications. Ann. Nutr. Metab. *77* (*Suppl 2*), 36–44. https://doi.org/10.1159/000516398.

18. Winek, K., Dirnagl, U., and Meisel, A. (2016). The gut microbiome as therapeutic target in central nervous system diseases: implications for stroke. Neurotherapeutics *13*, 762–774. https://doi.org/10.1007/s13311-016-0475-x.

19. Singh, V., Sadler, R., Heindl, S., Llovera, G., Roth, S., Benakis, C., and Liesz, A. (2018). The gut microbiome primes a cerebroprotective immune response after stroke. J. Cereb. Blood Flow Metab. *38*, 1293–1298. https://doi.org/10.1177/0271678X18780130.

20. Singh, V., Roth, S., Llovera, G., Sadler, R., Garzetti, D., Stecher, B., Dichgans, M., and Liesz, A. (2016). Microbiota dysbiosis controls the neuroinflammatory response after stroke. J. Neurosci. *36*, 7428–7440. https://doi.org/10.1523/JNEUROSCI.1114-16.2016.

21. Stanley, D., Moore, R.J., and Wong, C.H.Y. (2018). An insight into intestinal mucosal microbiota disruption after stroke. Sci. Rep. *8*, 568. https://doi.org/10.1038/s41598-017-18904-8.

22. Spychala, M.S., Venna, V.R., Jandzinski, M., Doran, S.J., Durgan, D.J., Ganesh, B.P., Ajami, N.J., Putluri, N., Graf, J., Bryan, R.M., and McCullough, L.D. (2018). Age-related changes in the gut microbiota influence systemic inflammation and stroke outcome. Ann. Neurol. *84*, 23–36. https://doi.org/10.1002/ana.25250.

23. Benakis, C., Brea, D., Caballero, S., Faraco, G., Moore, J., Murphy, M., Sita, G., Racchumi, G., Ling, L., Pamer, E.G., et al. (2016). Commensal microbiota affects ischemic stroke outcome by regulating intestinal gammadelta T cells. Nat. Med. *22*, 516–523. https://doi.org/10.1038/nm.4068.

24. Flint, H.J., Scott, K.P., Duncan, S.H., Louis, P., and Forano, E. (2012). Microbial degradation of complex carbohydrates in the gut. Gut Microb. *3*, 289–306. https://doi.org/10.4161/gmic.19897.

25. Lourbopoulos, A., Mamrak, U., Roth, S., Balbi, M., Shrouder, J., Liesz, A., Hellal, F., and Plesnila, N. (2017). Inadequate food and water intake determine mortality following stroke in mice. J. Cereb. Blood Flow Metab. *37*, 2084–2097. https://doi.org/10.1177/0271678X16660986.

26. Hughes, E.R., Winter, M.G., Duerkop, B.A., Spiga, L., Furtado de Carvalho, T., Zhu, W., Gillis, C.C., Büttner, L., Smoot, M.P., Behrendt, C.L., et al. (2017). Microbial respiration and formate oxidation as metabolic signatures of inflammation-associated dysbiosis. Cell Host Microbe *21*, 208–219. https://doi.org/10.1016/j.chom.2017.01.005.

27. Nam, H.S. (2019). Gut microbiota and ischemic stroke: the role of trimethylamine N-oxide. J. Stroke *21*, 151–159. https://doi.org/10.5853/jos.2019.00472.

28. Ilavenil, S., Arasu, M.V., Lee, J.C., Kim, D.H., Roh, S.G., Park, H.S., Choi, G.J., Mayakrishnan, V., and Choi, K.C. (2014). Trigonelline attenuates the adipocyte differentiation and lipid accumulation in 3T3-L1 cells. Phytomedicine *21*, 758–765. https://doi.org/10.1016/j.phymed.2013.11.007.

29. Stephens, T.W., Higgins, A.J., Cook, G.A., and Harris, R.A. (1985). Two mechanisms produce tissue-specific inhibition of fatty acid oxidation by oxfenicine. Biochem. J. *227*, 651–660. https://doi.org/10.1042/bj2270651.

30. Lo Verme, J., Fu, J., Astarita, G., La Rana, G., Russo, R., Calignano, A., and Piomelli, D. (2005). The nuclear receptor peroxisome proliferator-activated receptor-alpha mediates the anti-inflammatory actions of palmitoylethanolamide. Mol. Pharmacol. *67*, 15–19. https://doi.org/10.1124/mol.104.006353.

31. Mastrofrancesco, A., Ottaviani, M., Aspite, N., Cardinali, G., Izzo, E., Graupe, K., Zouboulis, C.C., Camera, E., and Picardo, M. (2010). Azelaic acid modulates the inflammatory response in normal human keratinocytes through PPARgamma activation. Exp. Dermatol. *19*, 813–820. https://doi.org/10.1111/j.1600-0625.2010.01107.x.

32. Mukherjee, R., Jow, L., Croston, G.E., and Paterniti, J.R., Jr. (1997). Identification, characterization, and tissue distribution of human peroxisome proliferator-activated receptor (PPAR) isoforms PPARgamma2 versus PPARgamma1 and activation with retinoid X receptor agonists and antagonists. J. Biol. Chem. *272*, 8071–8076. https://doi.org/10.1074/jbc.272.12.8071.

33. Sayin, S.I., Wahlström, A., Felin, J., Jäntti, S., Marschall, H.U., Bamberg, K., Angelin, B., Hyötyläinen, T., Orešič, M., and Bäckhed, F. (2013). Gut microbiota regulates bile acid metabolism by reducing the levels of tauro-beta-muricholic acid, a naturally occurring FXR antagonist. Cell Metab. *17*, 225–235. https://doi.org/10.1016/j.cmet.2013.01.003.

34. Sommer, F., Nookaew, I., Sommer, N., Fogelstrand, P., and Bäckhed, F. (2015). Site-specific programming of the host epithelial transcriptome by the gut microbiota. Genome Biol. *16*, 62. https://doi.org/10.1186/s13059-015-0614-4.

35. Vilà-Brau, A., De Sousa-Coelho, A.L., Mayordomo, C., Haro, D., and Marrero, P.F. (2011). Human HMGCS2 regulates mitochondrial fatty acid oxidation and FGF21 expression in HepG2 cell line. J. Biol. Chem. *286*, 20423–20430. https://doi.org/10.1074/jbc.M111.235044.

36. Trendelenburg, G., Prass, K., Priller, J., Kapinya, K., Polley, A., Muselmann, C., Ruscher, K., Kannbley, U., Schmitt, A.O., Castell, S., et al. (2002). Serial analysis of gene expression identifies metallothionein-II as major neuroprotective gene in mouse focal cerebral ischemia. J. Neurosci. *22*, 5879–5888.

37. Du, X., and Hu, H. (2021). The roles of 2-hydroxyglutarate. Front. Cell Dev. Biol. *9*, 651317. https://doi.org/10.3389/fcell.2021.651317.

38. Bilotta, A.J., Ma, C., Yang, W., Yu, Y., Yu, Y., Zhao, X., Zhou, Z., Yao, S., Dann, S.M., and Cong, Y. (2021). Propionate enhances cell speed and persistence to promote intestinal epithelial turnover and repair. Cell. Mol. Gastroenterol. Hepatol. *11*, 1023–1044. https://doi.org/10.1016/j.jcmgh.2020.11.011.

39. Okada, T., Fukuda, S., Hase, K., Nishiumi, S., Izumi, Y., Yoshida, M., Hagiwara, T., Kawashima, R., Yamazaki, M., Oshio, T., et al. (2013). Microbiota-derived lactate accelerates colon epithelial cell turnover in starvation-refed mice. Nat. Commun. *4*, 1654. https://doi.org/10.1038/ncomms2668.

40. Li, L., Sun, L., Qiu, Y., Zhu, W., Hu, K., and Mao, J. (2020). Protective effect of stachydrine against cerebral ischemia-reperfusion injury by reducing inflammation and apoptosis through P65 and JAK2/STAT3 signaling pathway. Front. Pharmacol. *11*, 64. https://doi.org/10.3389/fphar.2020.00064.

41. Lee, A.Y., and Chung, S.S. (1999). Contributions of polyol pathway to oxidative stress in diabetic cataract. FASEB J. *13*, 23–30. https://doi.org/10.1096/fasebj.13.1.23.

42. Stine, R.R., Sakers, A.P., TeSlaa, T., Kissig, M., Stine, Z.E., Kwon, C.W., Cheng, L., Lim, H.W., Kaestner, K.H., Rabinowitz, J.D., and Seale, P. (2019). PRDM16 maintains homeostasis of the intestinal epithelium by controlling region-specific metabolism. Cell Stem Cell *25*, 830–845.e8. https://doi.org/10.1016/j.stem.2019.08.017.

43. Mihaylova, M.M., Cheng, C.W., Cao, A.Q., Tripathi, S., Mana, M.D., Bauer-Rowe, K.E., Abu-Remaileh, M., Clavain, L., Erdemir, A., Lewis, C.A., et al. (2018). Fasting activates fatty acid oxidation to enhance intestinal stem cell function during homeostasis and aging. Cell Stem Cell *22*, 769–778.e4. https://doi.org/10.1016/j.stem.2018.04.001.

44. Zhu, X., Yan, J., Bregere, C., Zelmer, A., Goerne, T., Kapfhammer, J.P., Guzman, R., and Wellmann, S. (2019). RBM3 promotes neurogenesis in a niche-dependent manner via IMP2-IGF2 signaling pathway after hypoxic-ischemic brain injury. Nat. Commun. *10*, 3983. https://doi.org/10.1038/s41467-019-11870-x.

45. Lewington, A.J., Padanilam, B.J., and Hammerman, M.R. (1997). Induction of calcyclin after ischemic injury to rat kidney. Am. J. Physiol. *273*, F380–F385. https://doi.org/10.1152/ajprenal.1997.273.3.F380.

46. Chelikani, P.K., Haver, A.C., and Reidelberger, R.D. (2005). Intravenous infusion of peptide YY(3-36) potently inhibits food intake in rats. Endocrinology *146*, 879–888. https://doi.org/10.1210/en.2004-1138.

47. le Roux, C.W., and Bloom, S.R. (2005). Peptide YY, appetite and food intake. Proc. Nutr. Soc. *64*, 213–216. https://doi.org/10.1079/pns2005427.

48. Peterson, L.W., and Artis, D. (2014). Intestinal epithelial cells: regulators of barrier function and immune homeostasis. Nat. Rev. Immunol. *14*, 141–153. https://doi.org/10.1038/nri3608.

49. Kamada, N., Seo, S.U., Chen, G.Y., and Núñez, G. (2013). Role of the gut microbiota in immunity and inflammatory disease. Nat. Rev. Immunol. *13*, 321–335. https://doi.org/10.1038/nri3430.

50. Colliou, N., Ge, Y., Sahay, B., Gong, M., Zadeh, M., Owen, J.L., Neu, J., Farmerie, W.G., Alonzo, F., 3rd, Liu, K., et al. (2017). Commensal Propionibacterium strain UF1 mitigates intestinal inflammation via Th17 cell regulation. J. Clin. Invest. *127*, 3970–3986. https://doi.org/10.1172/JCI95376.

51. Ito, M., Komai, K., Mise-Omata, S., Iizuka-Koga, M., Noguchi, Y., Kondo, T., Sakai, R., Matsuo, K., Nakayama, T., Yoshie, O., et al. (2019). Brain regulatory T cells suppress astrogliosis and potentiate neurological recovery. Nature *565*, 246–250. https://doi.org/10.1038/s41586-018-0824-5.

52. Liesz, A., Suri-Payer, E., Veltkamp, C., Doerr, H., Sommer, C., Rivest, S., Giese, T., and Veltkamp, R. (2009). Regulatory T cells are key cerebroprotective immunomodulators in acute experimental stroke. Nat. Med. *15*, 192–199. https://doi.org/10.1038/nm.1927.

53. Zheng, D., Liwinski, T., and Elinav, E. (2020). Interaction between microbiota and immunity in health and disease. Cell Res. *30*, 492–506. https://doi.org/10.1038/s41422-020-0332-7.

54. Ma, Q., Xing, C., Long, W., Wang, H.Y., Liu, Q., and Wang, R.F. (2019). Impact of microbiota on central nervous system and neurological diseases: the gut-brain axis. J. Neuroinflammation *16*, 53. https://doi.org/10.1186/s12974-019-1434-3.

55. Chidambaram, S.B., Rathipriya, A.G., Mahalakshmi, A.M., Sharma, S., Hediyal, T.A., Ray, B., Sunanda, T., Rungratanawanich, W., Kashyap, R.S., Qoronfleh, M.W., et al. (2022). The influence of gut dysbiosis in the pathogenesis and management of ischemic stroke. Cells *11*. https://doi.org/10.3390/cells11071239.

56. Yilmaz, G., Arumugam, T.V., Stokes, K.Y., and Granger, D.N. (2006). Role of T lymphocytes and interferon-gamma in ischemic stroke. Circulation *113*, 2105–2112. https://doi.org/10.1161/CIRCULATIONAHA.105.593046.

57. Fung, C., and Vanden Berghe, P. (2020). Functional circuits and signal processing in the enteric nervous system. Cell. Mol. Life Sci. *77*, 4505–4522. https://doi.org/10.1007/s00018-020-03543-6.

58. Obata, Y., Castaño, Á., Boeing, S., Bon-Frauches, A.C., Fung, C., Fallesen, T., de Agüero, M.G., Yilmaz, B., Lopes, R., Huseynova, A., et al. (2020). Neuronal programming by microbiota regulates intestinal physiology. Nature *578*, 284–289. https://doi.org/10.1038/s41586-020-1975-8.

59. Schaller, B.J., Graf, R., and Jacobs, A.H. (2006). Pathophysiological changes of the gastrointestinal tract in ischemic stroke. Am. J. Gastroenterol. *101*, 1655–1665. https://doi.org/10.1111/j.1572-0241.2006.00540.x.

60. Stephens, J., Stoll, B., Cottrell, J., Chang, X., Helmrath, M., and Burrin, D.G. (2006). Glucagon-like peptide-2 acutely increases proximal small intestinal blood flow in TPN-fed neonatal piglets. Am. J. Physiol. Regul. Integr. Comp. Physiol. *290*, R283–R289. https://doi.org/10.1152/ajpregu.00588.2005.

61. Ogata, T., Kamouchi, M., Matsuo, R., Hata, J., Kuroda, J., Ago, T., Sugimori, H., Inoue, T., and Kitazono, T.; Fukuoka Stroke Registry (2014). Gastrointestinal bleeding in acute ischemic stroke: recent trends from the fukuoka stroke registry. Cerebrovasc. Dis. Extra *4*, 156–164. https://doi.org/10.1159/000365245.

62. Chen, Y., Liang, J., Ouyang, F., Chen, X., Lu, T., Jiang, Z., Li, J., Li, Y., and Zeng, J. (2019). Persistence of gut microbiota dysbiosis and chronic systemic inflammation after cerebral infarction in cynomolgus monkeys. Front. Neurol. *10*, 661. https://doi.org/10.3389/fneur.2019.00661.

63. Li, N., Wang, X., Sun, C., Wu, X., Lu, M., Si, Y., Ye, X., Wang, T., Yu, X., Zhao, X., et al. (2019). Change of intestinal microbiota in cerebral ischemic stroke patients. BMC Microbiol. *19*, 191. https://doi.org/10.1186/s12866-019-1552-1.

64. Koeth, R.A., Wang, Z., Levison, B.S., Buffa, J.A., Org, E., Sheehy, B.T., Britt, E.B., Fu, X., Wu, Y., Li, L., et al. (2013). Intestinal

microbiota metabolism of L-carnitine, a nutrient in red meat, promotes atherosclerosis. Nat. Med. *19*, 576–585. https://doi.org/10.1038/nm.3145.

65. Jung, J.Y., Lee, H.S., Kang, D.G., Kim, N.S., Cha, M.H., Bang, O.S., Ryu, D.H., and Hwang, G.S. (2011). 1H-NMR-based metabolomics study of cerebral infarction. Stroke *42*, 1282–1288. https://doi.org/10.1161/STROKEAHA.110.598789.

66. Mathewson, N.D., Jenq, R., Mathew, A.V., Koenigsknecht, M., Hanash, A., Toubai, T., Oravecz-Wilson, K., Wu, S.R., Sun, Y., Rossi, C., et al. (2016). Gut microbiome-derived metabolites modulate intestinal epithelial cell damage and mitigate graft-versus-host disease. Nat. Immunol. *17*, 505–513. https://doi.org/10.1038/ni.3400.

67. Fletcher, J.A., Deja, S., Satapati, S., Fu, X., Burgess, S.C., and Browning, J.D. (2019). Impaired ketogenesis and increased acetyl-CoA oxidation promote hyperglycemia in human fatty liver. JCI Insight *5*, 127737. https://doi.org/10.1172/jci.insight.127737.

68. Wang, Y.H., Liu, C.L., Chiu, W.C., Twu, Y.C., and Liao, Y.J. (2019). HMGCS2 mediates ketone production and regulates the proliferation and metastasis of hepatocellular carcinoma. Cancers *11*, E1876. https://doi.org/10.3390/cancers11121876.

69. Cheng, C.W., Biton, M., Haber, A.L., Gunduz, N., Eng, G., Gaynor, L.T., Tripathi, S., Calibasi-Kocal, G., Rickelt, S., Butty, V.L., et al. (2019). Ketone body signaling mediates intestinal stem cell homeostasis and adaptation to diet. Cell *178*, 1115–1131.e15. https://doi.org/10.1016/j.cell.2019.07.048.

70. Kim, J.T., Li, C., Weiss, H.L., Zhou, Y., Liu, C., Wang, Q., and Evers, B.M. (2019). Regulation of ketogenic enzyme HMGCS2 by wnt/beta-catenin/PPARgamma pathway in intestinal cells. Cells *8*. https://doi.org/10.3390/cells8091106.

71. Rodríguez, J.C., Gil-Gómez, G., Hegardt, F.G., and Haro, D. (1994). Peroxisome proliferator-activated receptor mediates induction of the mitochondrial 3-hydroxy-3-methylglutaryl-CoA synthase gene by fatty acids. J. Biol. Chem. *269*, 18767–18772.

72. Lei, W., Ren, W., Ohmoto, M., Urban, J.F., Jr., Matsumoto, I., Margolskee, R.F., and Jiang, P. (2018). Activation of intestinal tuft cell-expressed Sucnr1 triggers type 2 immunity in the mouse small intestine. Proc. Natl. Acad. Sci. USA *115*, 5552–5557. https://doi.org/10.1073/pnas.1720758115.

73. Kim, Y.S., and Ho, S.B. (2010). Intestinal goblet cells and mucins in health and disease: recent insights and progress. Curr. Gastroenterol. Rep. *12*, 319–330. https://doi.org/10.1007/s11894-010-0131-2.

74. Wei, M., Huang, Q., Liu, Z., Luo, Y., and Xia, J. (2021). Intestinal barrier dysfunction participates in the pathophysiology of ischemic stroke. CNS Neurol. Disord. Drug Targets *20*, 401–416. https://doi.org/10.2174/1871527320666210322115808.

75. Schneider, C., O'Leary, C.E., and Locksley, R.M. (2019). Regulation of immune responses by tuft cells. Nat. Rev. Immunol. *19*, 584–593. https://doi.org/10.1038/s41577-019-0176-x.

76. Crooks, B., Stamataki, N.S., and McLaughlin, J.T. (2021). Appetite, the enteroendocrine system, gastrointestinal disease and obesity. Proc. Nutr. Soc. *80*, 50–58. https://doi.org/10.1017/S0029665120006965.

77. Paquereau, J., Allart, E., Romon, M., and Rousseaux, M. (2014). The long-term nutritional status in stroke patients and its predictive factors. J. Stroke Cerebrovasc. Dis. *23*, 1628–1633. https://doi.org/10.1016/j.jstrokecerebrovasdis.2014.01.007.

78. Ladinsky, M.S., Araujo, L.P., Zhang, X., Veltri, J., Galan-Diez, M., Soualhi, S., Lee, C., Irie, K., Pinker, E.Y., Narushima, S., et al. (2019). Endocytosis of commensal antigens by intestinal epithelial cells regulates mucosal T cell homeostasis. Science *363*, eaat4042. https://doi.org/10.1126/science.aat4042.

79. Li, P., Gan, Y., Sun, B.L., Zhang, F., Lu, B., Gao, Y., Liang, W., Thomson, A.W., Chen, J., and Hu, X. (2013). Adoptive regulatory T-cell therapy protects against cerebral ischemia. Ann. Neurol. *74*, 458–471. https://doi.org/10.1002/ana.23815.

80. Park, S.G., Mathur, R., Long, M., Hosh, N., Hao, L., Hayden, M.S., and Ghosh, S. (2010). T regulatory cells maintain intestinal homeostasis by suppressing gammadelta T cells. Immunity *33*, 791–803. https://doi.org/10.1016/j.immuni.2010.10.014.

81. Shrestha, S., Yang, K., Guy, C., Vogel, P., Neale, G., and Chi, H. (2015). Treg cells require the phosphatase PTEN to restrain TH1 and TFH cell responses. Nat. Immunol. *16*, 178–187. https://doi.org/10.1038/ni.3076.

82. Hao, Y., Hao, S., Andersen-Nissen, E., Mauck, W.M., 3rd, Zheng, S., Butler, A., Lee, M.J., Wilk, A.J., Darby, C., Zager, M., et al. (2021). Integrated analysis of multimodal single-cell data. Cell *184*, 3573–3587.e29. https://doi.org/10.1016/j.cell.2021.04.048.

83. Li, S., Park, Y., Duraisingham, S., Strobel, F.H., Khan, N., Soltow, Q.A., Jones, D.P., and Pulendran, B. (2013). Predicting network activity from high throughput metabolomics. PLoS Comput. Biol. *9*, e1003123. https://doi.org/10.1371/journal.pcbi.1003123.

84. Bolyen, E., Rideout, J.R., Dillon, M.R., Bokulich, N.A., Abnet, C.C., Al-Ghalith, G.A., Alexander, H., Alm, E.J., Arumugam, M., Asnicar, F., et al. (2019). Reproducible, interactive, scalable and extensible microbiome data science using QIIME 2. Nat. Biotechnol. *37*, 852–857. https://doi.org/10.1038/s41587-019-0209-9.

85. Huang, D.W., Sherman, B.T., and Lempicki, R.A. (2009). Systematic and integrative analysis of large gene lists using DAVID bioinformatics resources. Nat. Protoc. *4*, 44–57. https://doi.org/10.1038/nprot.2008.211.

86. Yang, C., Yang, Y., DeMars, K.M., Rosenberg, G.A., and Candelario-Jalil, E. (2020). Genetic deletion or pharmacological inhibition of cyclooxygenase-2 reduces blood-brain barrier damage in experimental ischemic stroke. Front. Neurol. *11*, 887. https://doi.org/10.3389/fneur.2020.00887.

87. Ge, Y., Zadeh, M., and Mohamadzadeh, M. (2022). Vitamin B12 coordinates ileal epithelial cell and microbiota functions to resist Salmonella infection in mice. J. Exp. Med. *219*, e20220057. https://doi.org/10.1084/jem.20220057.

88. Kumar, A., Priyamvada, S., Ge, Y., Jayawardena, D., Singhal, M., Anbazhagan, A.N., Chatterjee, I., Dayal, A., Patel, M., Zadeh, K., et al. (2021). A novel role of SLC26A3 in the maintenance of intestinal epithelial barrier integrity. Gastroenterology *160*, 1240–1255.e3. https://doi.org/10.1053/j.gastro.2020.11.008.

89. Choi, S.C., Brown, J., Gong, M., Ge, Y., Zadeh, M., Li, W., Croker, B.P., Michailidis, G., Garrett, T.J., Mohamadzadeh, M., and Morel, L. (2020). Gut microbiota dysbiosis and altered tryptophan catabolism contribute to autoimmunity in lupus-susceptible mice. Sci. Transl. Med. *12*, eaax2220. https://doi.org/10.1126/scitranslmed.aax2220.

90. Ge, Y., Zadeh, M., and Mohamadzadeh, M. (2022). Vitamin B12 regulates the transcriptional, metabolic, and epigenetic programing in human ileal epithelial cells. Nutrients *14*, 2825. https://doi.org/10.3390/nu14142825.

91. Ge, Y., Gong, M., Zadeh, M., Li, J., Abbott, J.R., Li, W., Morel, L., Sonon, R., Supekar, N.T., Azadi, P., et al. (2020). Regulating colonic dendritic cells by commensal glycosylated large surface layer protein A to sustain gut homeostasis against pathogenic inflammation. Mucosal Immunol. *13*, 34–46. https://doi.org/10.1038/s41385-019-0210-0.

92. Butler, A., Hoffman, P., Smibert, P., Papalexi, E., and Satija, R. (2018). Integrating single-cell transcriptomic data across different conditions, technologies, and species. Nat. Biotechnol. *36*, 411–420. https://doi.org/10.1038/nbt.4096.

93. Haber, A.L., Biton, M., Rogel, N., Herbst, R.H., Shekhar, K., Smillie, C., Burgin, G., Delorey, T.M., Howitt, M.R., Katz, Y., et al. (2017). A single-cell survey of the small intestinal epithelium. Nature *551*, 333–339. https://doi.org/10.1038/nature24489.

94. Wang, Y., Song, W., Wang, J., Wang, T., Xiong, X., Qi, Z., Fu, W., Yang, X., and Chen, Y.G. (2020). Single-cell transcriptome analysis reveals differential nutrient absorption functions in human intestine. J. Exp. Med. *217*, e20191130. https://doi.org/10.1084/jem.20191130.

STAR★METHODS

KEY RESOURCES TABLE

REAGENT or RESOURCE	SOURCE	IDENTIFIER
Antibodies		
APC anti-mouse CD45	BioLegend	Cat# 103112 RRID;RRID:AB_312977
FITC anti-mouse CD31	BioLegend	Cat# 102406; RRID:AB_312901
PE/Cyanine7 anti-mouse TER-119	BioLegend	Cat# 116222; RRID:AB_2281408
APC/Cyanine7 anti-mouse CD3ε	BioLegend	Cat# 100330; RRID:AB_1877170
Brilliant Violet 605 anti-mouse CD4	BioLegend	Cat# 100548; RRID:AB_2563054
PerCP/Cyanine5.5 anti-mouse CD8α	BioLegend	Cat# 100734; RRID:AB_2075238
APC anti-mouse TCR γ/δ	BioLegend	Cat# 118116; RRID:AB_1731813
PE anti-mouse IL-17A	BioLegend	Cat# 506904; RRID:AB_315464
PE/Cyanine7 anti-mouse IFN-γ	BioLegend	Cat# 505826; RRID:AB_2295770
FITC anti-mouse IL-10	BioLegend	Cat# 505006; RRID:AB_315360
PE anti-mouse CD326 (EpCAM)	Thermo Fisher Scientific	Cat# 12-5791-83; RRID:AB_953617
Super Bright 645 anti-mouse CD45	Thermo Fisher Scientific	Cat# 64-0451-82; RRID:AB_2662420
eFluor 450 anti-mouse/rat FoxP3	Thermo Fisher Scientific	Cat# 48-5773-82; RRID:AB_1518812
Chemicals, peptides, and recombinant proteins		
FcR Blocking Reagent	Miltenyi Biotec	Cat# 130-092-575
True-Nuclear Transcription Factor Buffer Set	BioLgend	Cat# 424401
PowerUp SYBR Green Master Mix	Thermo Fisher Scientific	Cat# A25776
TrypLE Express	Thermo Fisher Scientific	Cat# 12604021
Critical commercial assays		
LIVE/DEAD Fixable Violet Dead Cell Stain Kit	Thermo Fisher Scientific	Cat# L34964
LIVE/DEAD Fixable Aqua Dead Cell Stain Kit	Thermo Fisher Scientific	Cat# L34966
Quick-DNA Fecal/Soil Microbe Miniprep Kit	Zymo Research	Cat# 11–322
RNeasy Plus Micro Kit	Qiagen	Cat# 74034
SMART-Seq HT Kit	Takara	Cat# 634438
Nextera XT DNA Library Preparation Kit	Illumina	Cat# FC-131-1096
Miseq Reagent Kit v3	Illumina	MS-102-3003
IDT for Illumina DNA/RNA UD Indexes	Illumina	Cat# 20026121
Chromium Next GEM Single Cell 5′ Reagent Kits v2 (Dual Index)	10X Genomics	Cat# PN-1000263
Deposited data		
Bulk RNA-seq	This paper	NCBI BioProject: PRJNA835890
Single-cell RNA-seq	This paper	NCBI BioProject: PRJNA880326
Experimental models: Organisms/strains		
C56BL/6J mice (male)	Jackson Laboratory	https://www.jax.org/
Oligonucleotides		
See Table S1 for primers used in this study		
Software and algorithms		
Cell Ranger	10X Genomics	N/A
Seurat v4.0.6	Hao et al.[82]	https://satijalab.org/seurat/
GraphPad Prism 9	GraphPad	N/A

(*Continued on next page*)

Continued

REAGENT or RESOURCE	SOURCE	IDENTIFIER
FlowJo v10	Treestar	N/A
Mummichog	Li et al.[83]	N/A
QIIME2	Bolyen et al.[84]	https://qiime2.org/
DAVID	Huang et al.[85]	https://david.ncifcrf.gov/
Other		
QuantStudio 6 Pro	Thermo Fisher Scientific	N/A
Cyto Aurora Flow cytometer	Cytek	N/A
SH800S Cell Sorter	Sony	N/A
Chromium Controller	10X Genomics	N/A

RESOURCE AVAILABILITY

Lead contact

Further information and requests for resources and reagents should be directed to and will be fulfilled by the lead contact, Mansour Mohamadzadeh (Zadehm@uthscsa.edu).

Materials availability

This study did not generate new unique reagents.

Data and code availability

Bulk RNA-seq and single-cell RNA-seq data have been made publicly available under the NCBI BioProject accession numbers: PRJNA835890, PRJNA880326. Accession numbers are listed in the key resources table.

This study did not generate original code.

Any additional information required to reanalyze the data reported in this paper is available from the lead contact upon request.

EXPERIMENTAL MODEL AND SUBJECT DETAILS

Animals

Specific-pathogen-free (SPF) C57BL/6J mice (male, 10–12 weeks old) were purchased from Jackson Laboratory and housed under 12 h of light per day in a temperature-controlled environment. All procedures were conducted in compliance with protocols approved by the Institutional Animal Care and Usage Committee (IACUC) of the University of Florida under the protocol numbers 202008484 and 201907934 and the Department of Laboratory Animal Resources of the University of Texas Health at San Antonio under protocol number 20210065AR.

METHOD DETAILS

Transient middle cerebral artery occlusion (MCAO) model

Ischemic stroke was induced by 45 min of intraluminal middle cerebral artery occlusion (MCAO).[86] Briefly, the mice were anaesthetized by gas inhalation in a chamber containing 1.5–2% isoflurane in 100% O_2. Once surgical levels of anesthesia were attained, animals were injected subcutaneously with 0.05 mg/kg of buprenorphine hydrochloride (Buprenex). Body temperature was maintained at 37°C by placing animals on a water-circulating heat pad (Gaymar, T/Pump) and temperature regulator with a rectal probe. Under microscopic magnification, the right common carotid artery, external carotid artery, and internal carotid artery (ICA) were exposed via a midline vertical incision in the neck. A 12-mm-long 6–0 silicone-coated nylon filament (Doccol, Cat. No. 602134) was advanced gently into the ICA approximately 9–10 mm from the carotid bifurcation until mild resistance was felt and cerebral blood flow was reduced by at least 75% of the baseline value, as assessed by laser Doppler flowmetry (moorVMS-LDF1 blood flow monitor, Moor Instruments). After 45 min of MCAO, the filament was gently retracted to allow reperfusion (confirmed by laser Doppler). The skin was closed, anesthesia discontinued, and the mice were allowed

to recover in a temperature-controlled chamber. Once mice recovered from anesthesia, they were placed in their home cages and a heating pad (Snuggle Safe brand) was place under the cage for the first 2 days after stroke. Buprenex was given subcutaneously every 12 h for pain relief along with 1 mL of warm saline. Sham-operated animals received the same surgical procedures except for the MCAO.

Gut microbiota analysis

16S rRNA libraries were constructed and sequenced as described previously.[87,88] Briefly, intestinal luminal contents and feces were collected from post-stroke and sham-operated mice at different time points after surgery. Genomic DNA was isolated using the Quick-DNA Fecal/Soil Microbe Miniprep Kit (Zymo Research). The 16S rRNA variable regions (v4-v5) were amplified, purified, and sequenced on an Illumina Miseq instrument using a Miseq Reagent kit v3 (Illumina). The obtained 2 × 300 bp paired-end reads were processed using QIIME 2 (version 2020.8). Reads were merged, quality trimmed and clustered into operational taxonomic units (OTUs) at 97% sequence similarity. Taxonomy was assigned using Greengenes 13_8. To estimate within sample richness, α-diversity was determined using Shannon index. To evaluate differences in diversity across samples, β-diversity was determined using unweighted UniFrac distances. Differences in relative abundance at different taxonomic levels were determined using Mann-Whitney *U*-test.

Metabolomic analysis

Samples were homogenized in ammonium acetate, and proteins were pelleted after adding a mixture of acetonitrile, methanol, and acetone.[89] After centrifugation, the supernatants were transferred to a clean tube and dried under a gentle stream of nitrogen before reconstitution in formic acid-water solution. Metabolites were analyzed at the Southeast Center for Integrated Metabolomics (www.secim.ufl.edu) using a Thermo Q-Exactive Oribtrap mass spectrometer with Dionex UHPLC and autosampler.[87,90] Samples were run in both positive and negative ionization with a mass resolution of 35,000 at m/z 200. Feature alignment and curation were performed by MZmine through an automated routine developed in-house. After normalizing to total ion chromatogram (TIC), intensities were tested for group significance using unpaired Student *t*-test. For fecal metabolite, the p-values were adjusted for multiple comparisons based on Benjamini, Krieger and Yekutieli false discovery rate (FDR) correction at 1%. Metabolites were identified by comparison to metabolomic library of purified standards. Metabolic pathway analysis was performed using *Mummichog* with default parameters (http://mummichog-2.appspot.com/). The pathways represented by at least 2 significant metabolites in positive or negative mode are presented.

Isolation of epithelial cells (ECs)

The ileum (similar length as colon moving proximal from the ileocecal junction), cecum and colon were dissected from mice after MCAO or sham surgery. After washing with cold PBS, the tissues were opened longitudinally and cut into small fragments (2–3 cm in length), followed by incubation with 30 mM EDTA-PBS on ice for 30 min, during which the tissues were shaken vigorously every 8–10 min. Isolated crypts were washed once with cold PBS and dissociated using TrypLE Express (Invitrogen) for 10 min at room temperature. Cell suspensions were passed through a 70-μm cell strainer and then labeled with a cocktail of fluorescent antibodies specific for APC-CD45 (Invitrogen, catalog 17-0451-83), FITC-CD31 (BioLegend, catalog 102406), PE/Cy7-TER-119 (BioLegend, catalog 116222), and PE-EpCAM (Invitrogen, catalog 12-5791-83). Dead cells were excluded using LIVE/DEAD Fixable Violet Dead Cell Stain (Invitrogen). $CD45^-$ $CD31^-$ $TER\text{-}119^-$ $EpCAM^+$ ECs were sorted using a SONY SH800S Cell Sorter.

Bulk RNA-seq

Total RNA was extracted from FACS-sorted ECs (about 1×10^5 cells) isolated from each individual mouse using an RNeasy Plus Micro Kit (Qiagen). cDNA was generated using a SMART-Seq HT kit (Takara) and RNA-Seq libraries were constructed using a Nextera XT DNA Library Preparation Kit (Illumina).[87,91] The barcoded RNA-seq libraries were sequenced on an Illumina NovaSeq 6000 system at the University of Florida ICBR NextGen DNA sequencing Core Facility, with a minimal depth of 32 million reads/sample (2 × 150 bp). Obtained raw reads were aligned to the mouse reference genomes (GRCm38) using STAR v2.7.5c. Normalized counts (FPKM) were generated using RSEM v1.3.3. DESeq2 was used to determine significantly expressed genes (DEGs) based on the criteria (FPKM >1, FDR <0.05, fold change >1.5). FPKM values were used for principal component analysis (PCA) and plotting heat maps in R. Gene set

enrichment analysis (GSEA) was performed using DAVID (https://david.ncifcrf.gov/). Network analysis using STRING version 11.5 was performed for the overlapped DEGs using default parameters.

Single-cell RNA-seq

$CD45^-$ $CD31^-$ TER-119^- $EpCAM^+$ iECs were FACS-sorted from post-stroke and sham-operated mice one day after the surgery as described above. The purified iECs (75–85% viability) were processed using the Chromium single cell gene expression platform (10x Genomics). iECs isolated from each mouse were directly loaded into each sample well following manufacturer's instructions and combined into droplets with barcoded beads using the Chromium controller. Libraries were constructed using the Chromium Next GEM Single Cell 5' Reagent Kits v2 (10x Genomics) per manufacturer's instructions. The samples were sequenced to an average depth of 44,000–64,000 reads per cell on an Illumina NovaSeq 6000 sequencer.

Sequence reads were processed using the Cell Ranger 6.0.1 pipeline and aligned to the GRCm38 (mm10) mouse reference genome. The exonic reads uniquely mapped to the transcriptome were then used for unique molecular identifier (UMI) counting. Using Seurat (v4.0.6) R package,[92] cells that contained fewer than 500 or more than 7000 genes (nFeature_RNA), less than 800 or more than 60,000 molecules (nCount_RNA), or more than 10% mitochondrial transcripts (percet.mt) were removed. For each cell, expression of each gene was normalized to the sequencing depth of the cell, scaled to a constant depth (10,000), and log-transformed. Variable genes were selected using default parameters. Principal component analysis (PCA) was performed on the variable genes, and 15 principal components (PCs) were chosen based on elbow plots and jackstraw resampling. Samples of each condition were merged, and the two conditions (sham and stroke) were integrated using reciprocal PCA. Dimensionality reduction and visualization were performed with the UMAP algorithm, and unsupervised clustering of cells was performed using 15 PCs as defined above, with a resolution of 0.3. To identify signature genes of each cell cluster, the FindAllMarkers() function in Seurat was used with the following configurations: min.pct = 0.25, logfc.threshold = 0.585, only.pos = TRUE. An expression heatmap was generated for each sample by selecting the top 10 genes, which were used to define different cell populations by comparing them to known marker genes.[93,94] To identify differentially expressed genes in each cell type across the two different conditions, the integrated Seurat object was split into different cell subpopulations using the subset() function and differential analysis was performed using FindMarkers() function.

qRT-PCR

For validating DEGs identified by RNA-Seq, cDNA samples that were synthesized with SMART-Seq HT Kit (Takara) to construct RNA-seq libraries were used. Quantitative real-time PCR was performed with the PowerUp SYBR Green Master Mix (Thermo Fisher) on a QuantStudio 6 Pro real-time PCR system (Thermo Fisher). The relative quantification ($2^{-\Delta Ct}$) was used to determine the expression level of the target genes normalized *Gapdh*. Sequences of primers can be found in Table S1.

Flow cytometry

Immune cells were isolated from the ileum, cecum and colon of post-stroke and sham mice and analyzed by flow cytometry.[91] Dead cells were detected using LIVE/DEAD® Fixable Aqua Dead Cell Stain Kit (Thermo Fisher Scientific). Cell surface and intracellular markers were stained with following fluorescent antibodies: Super Bright 645-CD45 (catalog 64-0451-82) from Invitrogen and APC/Cy7-CD3 (catalog 100330), Brilliant Violet 605-CD4 (catalog 100548), PerCP/Cy5.5-CD8 (catalog 100734), APC-TCR γ/δ (catalog 118116), PE-IL-17A (catalog 506904), PE/Cy7-IFNγ, FITC-IL-10 (catalog 505006), eFluor450-FoxP3 (catalog 48-5773-82) from BioLegend. Data were collected by a Cytek Aurora flow cytometer and analyzed with FlowJo software (v10.8.1). After dead and doublet cell exclusion and $CD45^+$ live cell selection, γδ T cells were defined as $CD3^+$ $CD4^-$ TCR γ/δ^+ and CD4 T cells as $CD3^+$ $CD8^-$ $CD4^+$.

QUANTIFICATION AND STATISTICAL ANALYSIS

Statistical analyses were performed using GraphPad Prism v9.1.2. Prior to statistical analysis, normality was tested using the Shapiro-Wilk normality test. Where the groups follow a Gaussian distribution, two-tailed unpaired Student *t*-test was performed. Where the groups did not follow a Gaussian distribution, Mann–Whitney *U* test was performed. $p < 0.05$ were considered as significant: *, $p < 0.05$; **, $p < 0.01$; ***, $p < 0.001$; ****, $p < 0.0001$.